HELSINKI UNIVERSITY OF TECHNOLOGY
Department of Electrical and Communications Engineering

Aki Silvennoinen

RADIO CHANNEL MODELLING IN DIFFERENT OUTDOOR ENVIRONMENTS FOR WLAN SYSTEMS

Thesis submitted in partial fulfilment of the requirements for the degree of Master of Science in Technology in Espoo November 27th, 2003

Supervisor Professor Sven-Gustav Häggman

Instructor Michael Hall Lic.Sc.(Tech.)

HELSINKI UNIVERSITY OF TECHNOLOGY

Abstract of the Master's Thesis

Author:	Aki Silvennoinen
Name of the thesis:	Radio Channel Modelling in Different Outdoor Environments for WLAN Systems
Date:	November 27th 2003 **Number of pages:** 92
Department:	Department of Electrical and Communications Engineering
Professorship:	Communications Engineering
Supervisor:	Professor Sven-Gustav Häggman
Instructor:	Michael Hall Lic. Sc. (Tech.)

In this Master's thesis the process of radio channel modelling in different outdoor environments for WLAN systems is investigated. The means of the study was literature research and empirical measurements for testing of possible measurement equipment.

The first part of the thesis presents different WLAN techniques and their characteristics in the sense of channel modelling. Next, the basic radio wave propagation phenomena and existing large-scale and small-scale channel models are presented. The review of large-scale models concentrates on outdoor models outside urban environment and propagation in vegetation. Small-scale models cover the system functions of linear time-variant channels to existing tapped delay line models developed. Methods of actual channel modelling are presented next. The methods are divided into computer-aided propagation prediction and empirical channel modelling methods. Finally, the methods are applied to WLAN systems and environments that were a subject of this thesis.

The lack of suitable and accurate existing channel models for required environments and frequency band results in a need for carrying out the channel modelling personally. Also computer-aided propagation prediction methods proved inappropriate for the purposes of this thesis, which leads to the need for a heavy channel measurements campaign using expensive channel sounder equipment.

WLAN signal characteristics prevent measurements of channels with larger delay spread than 1 μs (IEEE 802.11, 727ns for IEEE 802.11b). Therefore, WLAN signals are unsuitable for channel measurements and a more general perspective should be taken. This characteristic also has a major impact on WLAN system behaviour at 2.4 GHz, since the receiver is incapable of receiving components arriving later than this delay without advanced countermeasures.

Keywords: Radio channel modelling, radio wave propagation, WLAN

TEKNILLINEN KORKEAKOULU

Diplomityön tiivistelmä

Tekijä:	Aki Silvennoinen
Työn nimi:	Radiokanavan mallinnus erilaisissa ympäristöissä ulkoilmassa WLAN järjestelmässä
Päivämäärä:	27. marraskuuta 2003 **Sivumäärä:** 92
Osasto:	Sähkö- ja tietoliikennetekniikan osasto
Professuuri:	Tietoliikennetekniikka
Työn valvoja:	Professori Sven-Gustav Häggman
Työn ohjaaja:	TkL Michael Hall

Tässä diplomityössä tutkittiin WLAN järjestelmän käyttämän radiokanavan mallinnusprosessia erilaisissa ulkoilmaympäristöissä. Tutkimusmenetelmiä olivat kirjallisuustutkimus sekä empiiriset mittaukset, joilla kokeiltiin erään potentiaalisen mittalaitteiston soveltuvuutta.

Diplomityön ensimmäisessä osassa esitellään erilaisia WLAN tekniikoita sekä niiden erityispiirteitä kanavamallinnuksen kannalta. Seuraavassa osassa esitellään radioaaltojen etenemisen perusilmiötä sekä olemassa olevia laajamittaisia ja pienimuotoisia kanavamalleja. Laajamittaisten mallien tarkastelu keskittyy ulkoilmaympäristöihin kaupunkialueiden ulkopuolella sekä kasvillisuus-etenemiseen. Pienimuotoisten mallien käsittely sisältää asiaa lineaaristen aikariippuvien kanavien systeemifunktioista olemassaoleviin viivästettyjen tappien linjamalleihin. Myös varsinaisen kanavamallinnuksen menetelmiä käydään läpi. Nämä menetelmät jakautuvat tietokoneavusteisiin ennustuksiin sekä empiirisiin kanavamallinnusmenetelmiin. Lopuksi menetelmiä sovelletaan WLAN järjestelmiin mainittuihin ympäristöihin.

Oikealla taajuuskaistalla olevien vaadittuihin ympäristöihin soveltuvien kanavamallien puutteesta johtuen on tarpeellista toteuttaa kanavanmallinnus itse. Myös tietokoneavusteisiin ennustuksiin perustuvat menetelmät osoittautuivat tämän työn tavoitteiden kannalta soveltumattomiksi, joten on tarpeellista toteuttaa raskas kanavanmittauskampanja käyttäen kallista kanavaluotain-järjestelmää.

WLAN signaalin erityispiirteet rajoittavat mittauksia kanavassa, jonka viivehaje on suurempi kuin 1μs (IEEE 802.11, 727ns IEEE 802.11b:lle) . Tämän johdosta WLAN signaali ei ole soveltuva kanavamittauksiin, vaan on tarpeellista ottaa yleisempi näkökulma. Tämä erityispiirre on vaikuttaa myös merkittävästi WLAN järjestelmän toimintaan 2,4 GHz:n taajuusalueella, sillä vastaanotin ei kykene vastaanottamaan signaalikomponentteja, jotka saapuvat mainuttua viivettä myöhemmin mikäli edistyksellisiä vastakeinoja ei ole käytössä.

Avainsanat:	Radiokanavan mallinnus, radioaaltojen eteneminen, WLAN

Preface

This thesis was carried out in the Communications Laboratory of Helsinki University of Technology as a part of a larger research project funded by the Finnish Defence Forces.

I would like to thank my Supervisor Prof. Sven-Gustav Häggman for all the advice, comments and inspiring guidance that helped to carry out this work. Without his support it would not have been possible to accomplish this thesis.

I am grateful to my Instructor, Lic. Sc. Michael Hall for his endless help clearing out basic facts and especially for the support in English grammar.

I would also like to thank the research group, Jukka, Petri and Teemu, for putting up with me and my silly questions. They have been very helpful and great workmates. Special thanks also to Lasse Vuokko of the Radio laboratory for exclusive information of a radio channel sounder equipment.

Finally, I want to express my thanks to Riitta for all the support especially during this thesis, and to my mom Mervi for supporting and giving me courage throughout my studies.

In Otaniemi, Espoo
November 27th 2003

Aki Silvennoinen

Table of contents

Abbreviations

AGC	Automatic Gain Control
AP	Access Point
BER	Bit Error Ratio
BS	Base Station
BSS	Basic Service Set
CCK	Complementary Code Keying
CFP	Contention-Free Period
COST	European Co-operation in the field of Scientific and Technical Research
CP	Contention Period
CSMA/CA	Carrier Sense Multiple Access with Collision Avoidance
CSMA/CD	Carrier Sense Multiple Access with Collision Detection
CTS	Clear To Send
CW	Continuous Wave
DCF	Distributed Coordination Function
DS	Distribution System
DSSS	Direct Sequence Spread Spectrum
EIRP	Equivalent Isotropically Radiated Power
ESS	Extended Service Set
ETSI	European Telecommunications Standards Institute
FDDI	Fibre Distributed Data Interface
FDTD	Finite Difference Time-Domain
FEM	Finite-Element Method
FER	Frame Error Ratio
FHSS	Frequency Hopping Spread Spectrum
HR/DSSS	High-Rate Direct Sequence Spread Spectrum
IBSS	Independent Basic Service Set
IF	Intermediate Frequency
IR	Infrared

ISI	Intersymbol Interference
ITU	International Telecommunications Union
LAI	Leaf Area Index
LOS	Line-Of-Sight
LTV	Linear Time-Variant
MAC	Medium Access Control
MAN	Metropolitan Area Network
MS	Mobile Station
NLOS	Non-Line-Of-Sight
OFDM	Orthogonal Frequency Division Multiplexing
PCF	Point Coordination Function
PDF	Probability Density Function
PDP	Power Delay Profile
PHY	Physical Layer
PN	Pseudo-Noise
RET	Radiative Energy Transfer
RF	Radio Frequency
RMS	Root Mean Square
RTS	Request To Send
RX	Receiver
SC	Sliding Correlator
SNR	Signal-To-Noise Ratio
TX	Transmitter
U-NII	Unlicensed National Information Infrastructure
UMTS	Universal Mobile Telecommunication Services/System
W-I	Walfisch-Ikegami propagation channel model
WLAN	Wireless Local Area Network
WSSUS	Wide-Sense Stationary Uncorrelated Scattering

List of symbols

α	Angle Between Speed Vector and Arriving Wave
α	Ratio of Forward Scattered Power to the total Scattered Power
$\alpha_n(t)$	Gain of the nth propagation path
β	Beamwidth of the Phase Function
$\Delta\gamma_R$	Beamwidth of the Receiving Antenna
ε	Permittivity of the Material
θ_g	Grazing Angle
λ	Wavelength
γ	Specific attenuation for very short vegetative paths (dB/m)
μ	Permeability of the Material
σ	Standard Deviation
$\sigma(t)$	Time-varying Standard Deviation
σ_c	Combined Absorption and Scatter Coefficient
σ^2	Time-average Power of the Received Signal
τ	Decay Factor
τ	Delay Variable
τ	Optical Density
$\tau_n(t)$	Propagation Delay of the nth Propagation Path
$\Delta\tau$	Unit Tap Delay
φ	Road Orientation with the Respect to the Direct Radio Path
$\Gamma_{\perp,\parallel}$	Reflection Coefficient: Perpendicular, Parallel Polarisation
X_σ	Zero-mean Gaussian Distributed Random Variable
A	Peak Amplitude of the Signal
A_e	Antenna Cross Section
A_{ev}	Excess attenuation
A_m	Maximum attenuation for one terminal within a specific type and depth of vegetation (dB)

b	Building Separation
B	Bandwidth
B_D	Doppler-spread
B_m	Coherence Bandwidth
d	Distance Between Transmitter and Receiver
d	Distance into the Vegetation in Metres
d_0	Reference Distance
d_{veg}	Total Vegetation Depth
D	Mean Excess Delay
$D(f,v)$	Output Doppler-Spread Function
f_c	Carrier Frequency
f_{chip}	Chip Rate
f_D	Doppler Shift
$f_{D,\max}$	Maximum Doppler Frequency
G_{TX}	Antenna Gain
h_{BS}	Base Station Antenna Height
h_{MS}	Mobile Station Antenna Height
$h_k(t)$	Complex Time-variant Tap Coefficients
h_{roof}	Building Heights
$h(\tau,t)$	Time-Variant Impulse Response
$H(f,t)$	Time-Variant Transfer Function
I_0	Modified Bessel Function of the First Kind and Zero Order
K	Ricean Factor
K	Scaling Factor
L	Path Loss
L_0	Free Space Loss
L_c	Loss Correction Term

L_{ground}	Ground-reflected Component Loss
L_{msd}	Multiple Screen Diffraction Loss
L_{rts}	Roof-to-Street Diffraction and Scatter Loss
L_{ori}	Street Orientation Loss
L_{side}	Side-diffracted Component Loss
L_{top}	Top-diffracted Component Loss
m	Number of Delay Element
n	Path Loss Exponent
P_0	Peak power (dB)
$P_D(0,v)$	Doppler Power Spectrum
$P_h(\tau,0)$	Multipath Intensity Profile / Delay Power Spectrum
$P_H(\Delta f,0)$	Frequency Correlation Function
$P_H(0,\Delta t)$	Time Correlation Function
$p(r)$	Probability Density Function
$P(\tau_m)$	Power Delay Profile
P_{TX}	Transmitted Power
r	Radius
r	Rayleigh Fading Signal Envelope
$r/2$	Short-term Signal Power
$r(t)$	Received Complex Baseband Signal
R_0	Ground Reflection Coefficient
R_s	Symbol Rate
$R_s(\tau)$	Autocorrelation Function
S	RMS Delay Spread
S	Power Density
t	Time
$T_{\perp,\parallel}$	Penetration Coefficient: Perpendicular, Parallel Polarisation

T_D	Coherence Time
T_m	Delay Spread
T_S	Simulation System Sampling Interval
T_S	Symbol Duration
V	Velocity
Δv	Frequency Shift Variable
w	Width of the Roads
$w(t)$	Time Domain Function
W	Reflectance (or Albedo)
$W(f)$	Frequency Domain Function

1. Introduction

In recent years the need for broadband internet access has grown rapidly, and the Internet with its services has become a part of common people's everyday life. This need is reflected as a supply and development of various types of communication systems, both wireless and wired. Wireless local area network (WLAN) is one the most successful systems developed due to its low investment costs and its usage of license-free frequency band.

The development of WLAN systems is leading towards higher and higher transferred data rates, which are using more and more complex modulation methods. Complex modulation methods make the systems more sensitive to interference particularly intersymbolic interference (ISI) caused by multipath propagation. Therefore, there is a great need for detailed radio channel information to be able to understand and compensate communication quality degradation by countermeasures.

IEEE 802.11b WLAN system operates in the license-free 2.4 GHz frequency band. Due to the popularity of IEEE 802.11b, the 2.4 GHz frequency band has been researched quite a lot. The channel characteristics in indoor and urban city environments are quite well known and different channel modelling results are available in the books and scientific journals (for reference, see p. 41). However, the low investment costs and easy usage of the system has generated interest in using the system also outside its traditional operating environments, e.g. outdoors, outside urban city environments. As far as the propagating radio channel is concerned, such environments display very different propagation conditions due e.g. vegetation, large delay spreads and perhaps fewer multipath components.

The purpose of this thesis is to find out the process of determining wideband radio channel models for WLAN systems in different outdoor environments. The main focus is on IEEE 802.11b WLAN system. The research is a first step in determining the characteristics of the propagating radio channel and applying this information to conclude how well WLAN can be used outdoors in different environments and what is the environment's impact on WLAN system. The means of this research are literature research and empirical measurements. The measurements were conducted to determine whether an inexpensive commercial measurement tool is suitable for channel modelling purposes.

In Chapter 2 of this thesis different WLAN techniques and their characteristics are presented. Even though other systems are also included, the focus is on IEEE 802.11b. Chapter 3 inspects basic radio wave propagation mechanisms. These mechanisms are the basics upon which more complicated channel

models are being developed. In Chapter 4, suitable existing channel models are presented. The focus is on outdoor environments outside urban cities and on propagation in vegetation. Large-scale models include distance path loss and shadowing loss models, whereas small-scale models are more accurate and based on system functions of linear time-variant channel. Chapter 5 investigates different channel modelling methods in a general perspective and Chapter 6 consists of applying these channel modelling methods to WLAN systems. The conclusions of the thesis are drawn in the last chapter.

2. Wireless LAN techniques and their characteristics

Wireless computing has been a rapidly growing technology already for many years. Wireless local area networks (WLAN) provide users with network connectivity just as wired networks do. WLAN provides high bandwidth to users in a limited area over the radio path. In this chapter relevant wireless LAN techniques are presented. The main emphasis is on WLAN systems that operate in the 2.4 GHz frequency band but some other systems are also given a general view.

2.1. IEEE 802.11

IEEE 802.11 is an international standard for WLAN systems. Nowadays, it can perhaps be regarded as the basic WLAN standard that the newer versions are based on. IEEE 802.11 describes the functionality and relationships between the two lowest layers in the OSI model; the physical layer (PHY) and the medium access control (MAC) sublayer. The standard does not specify how the functionality is to be implemented and this is left to manufacturers. The basic layer structure of the standard is shown in Figure 1 [San01, p.46].

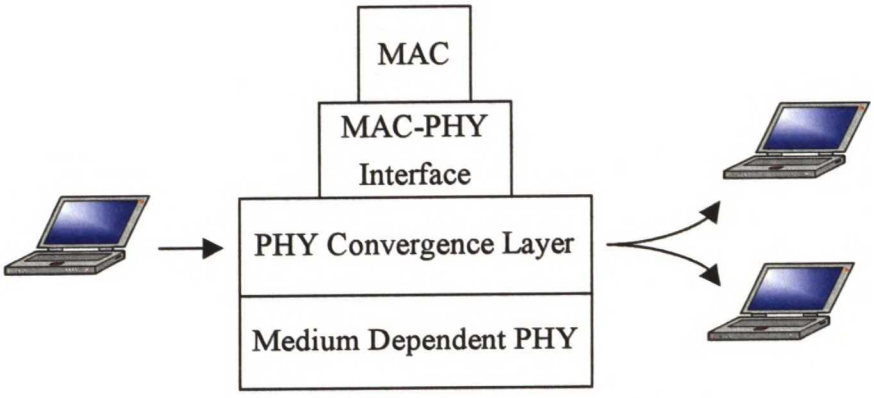

Figure 1 Basic layer structure of the IEEE 802.11 standard.

The IEEE 802.11 standard defines two alternative ways of implementing a WLAN network; terminals (station, STA) are connected only to each other inside an independent basic service set (BSS) and terminals are connected to a backbone network through an access point (AP) [IEE99a, p.11]. IEEE 802.11 is part of the IEEE 802 family and the MAC layer has similarities with the Ethernet, IEEE 802.3. IEEE 802.11 uses packet switched data with a nominal bit rate of mandatory 1 Mbit/s and optionally 2 Mbit/s. The network can be used for time-bounded traffic e.g. packetized voice and video and asynchronous data that is time insensitive, e.g. email and file transfers [Cro97, p.116].

2.1.1. Network topologies

Basic service set (BSS) is a basic building element of the IEEE 802.11 architecture. BSS is defined as a group of stations that are under the direct control of a single coordination function (i.e. distributed coordination function (DCF) or point coordination function (PCF)) [Cro97, p.117]. There are three main types of network topologies: Independent BSS (IBSS), Infrastructure BSS and Extended Service Set (ESS) [Gas02, pp.10-11].

Independent BSS (IBSS)

IBSS (often referred to as ad-hoc networks) is the deliberate grouping of stations into a single BSS for the purpose of internetworked communications without the aid of an infrastructure network. Stations in an IBSS communicate directly with each other within the direct communication range. IBSS is shown in Figure 2 (a) [Cro97, pp.117-118].

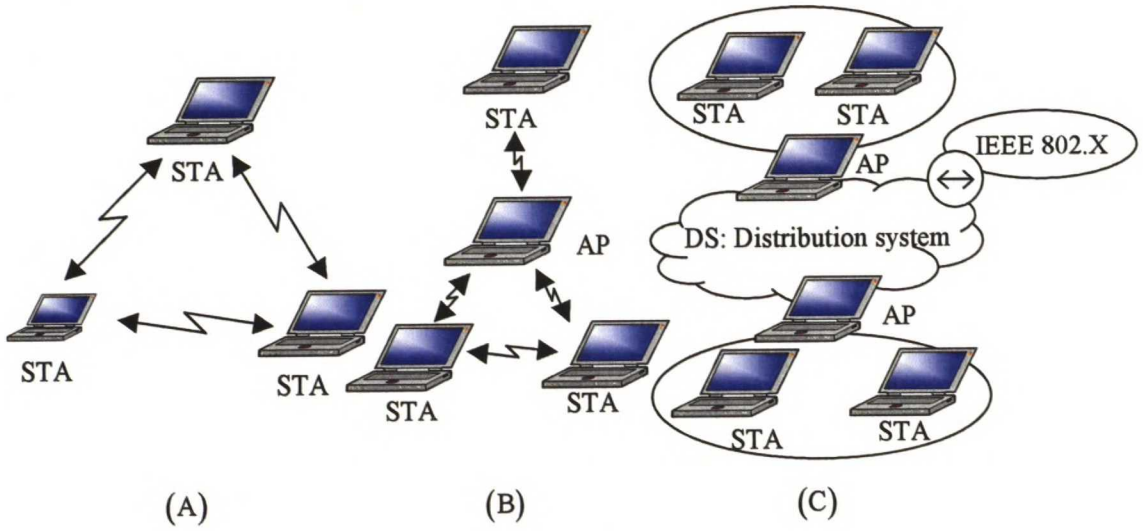

Figure 2 Network topologies: (a) Independent BSS, (b) Infrastructure BSS, and (c) ESS.

Infrastructure BSS

Infrastructure BSS is distinguished from IBSS only by the use of an access point (AP). AP is used for all communication in infrastructure networks, including communication between mobile nodes in the same area [Gas02, p.11]. The infrastructure BSS area is defined by the coverage distance from AP. AP can be connected to the backbone network and provides e.g. Internet access to wireless users through a gateway. Infrastructure BSS is shown in Figure 2 (b).

Extended Service Set (ESS)

ESS is used to cover larger areas with WLAN radio networks since BSSs can only cover a limited area. In ESS, several BSSs are linked to each other with a

backbone network called a distribution system (DS). The DS, as specified in IEEE 802.11, is implementation independent and therefore it could be e.g. any 802.X, fibre distributed data interface (FDDI) or metropolitan area network (MAN). An ESS can also provide gateway access for wireless users into a wired network e.g. the Internet. This is done through a device called a portal. ESS is shown in Figure 2 (c).

2.1.2. Medium access control (MAC)

There are two possibilities for MAC schemes specified in IEEE 802.11: distributed coordination function (DCF) and point coordination function (PCF). The MAC can also alternate between contention modes, known as contention period (CP) and contention-free period (CFP). MAC architecture is presented in Figure 3, where it is shown that the DCF sits directly on top of the physical layer [Cro97, p.119]. PCF is required to coexist with the DCF and logically sits on top of DCF.

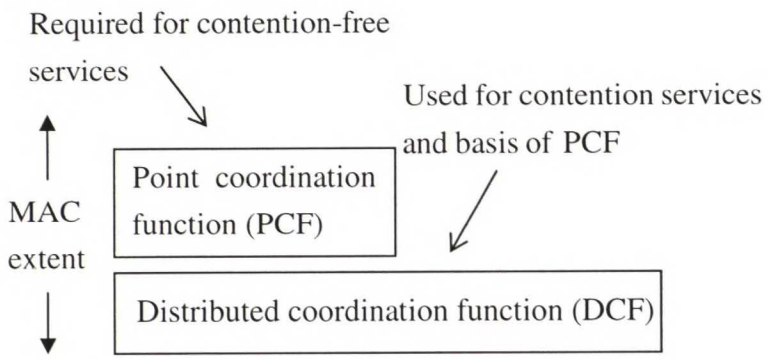

Figure 3 MAC architecture.

Distributed coordination function (DCF)

DCF is similar to traditional packet networks supporting best effort delivery of data. DCF is designed for asynchronous data transfer where all terminals with transferable data have an equal chance of accessing the network.

DCF is based on carrier sense multiple access with collision avoidance (CSMA/CA). Carrier sensing can be carried out either physically or virtually. In physical carrier sensing the station listens to the channel over the air interface. The channel is assumed clear if no other IEEE 802.11 WLAN carrier is present [Cro97, p.119]. This is a simple procedure and it is not very efficient in collision avoidance e.g. there are problems in detecting a Hidden Station. The Hidden Station problem occurs when an STA is located so that it is accessing AP but out of reach of another STA performing carrier sensing and therefore not detected. Virtual carrier sensing is performed by the MAC sublayer and it is based on the use of Request To Send (RTS) and Clear To Send (CTS) frames.

Here the STA sends first the RTS-frame to AP and the channel is assumed clear only if the CTS-frame is received from AP. This procedure is more complex and RTS/CTS-frames also consume the data transfer resources, but collision avoidance is more efficient, which may lead to better network efficiency [Chh96, p.14]. When using virtual carrier sensing, Network Allocation Vectors (NAV) are also used. NAVs tell the users how much time an upcoming transmission needs. During the DCF period the contention period (CP) is always used.

Point coordination function (PCF)

PCF is connection orientated and it is designed for the transmission of delay-sensitive traffic. It is based on polling that is controlled by AP. AP keeps a polling list and assigns timeslots for users that are connected. IEEE 802.11 also leaves the polling procedure implementation independent. PCF and DCF schemes can also be used together for combined performance. In this case MAC operates a while in PCF mode and then another while in DCF mode. During the PCF period, a contention-free period (CFP) can also be used.

2.1.3. Physical layer (PHY)

There are two specifications for radio systems within the IEEE 802.11 physical layer: frequency hopping spread spectrum (FHSS) and direct sequence spread spectrum (DSSS). A specification of infrared (IR) also exists in the standard but is outside the scope of this thesis and therefore it is not dealt with. Both FHSS and DSSS use spread spectrum techniques and operate in the unlicensed 2.4 GHz ISM (Industrial, Scientific, Medical) band that is available in many parts of the world. For most countries, including Finland, the 2.4 GHz ISM band ranges from 2.4 to 2.4835 GHz [Vie03]. Radio frequency (RF) challenges of the 2.4 GHz ISM band are considered more deeply in Section 2.5.

Spread spectrum techniques

Spread spectrum systems use more bandwidth than is needed for transmission. This is achieved by using a spreading code in the transmitter prior to the modulator. The code differs from the transmitted data and it must be known by the receiver otherwise the receiver cannot decode the data. When comparing spread spectrum wideband signal with narrowband transmissions, spread spectrum transmissions are more difficult to detect, intercept or decode. Also they are less sensitive to interference from other users and less likely to interfere with others [San01, p.71]. Frequency hopping and direct sequence are typical spread spectrum techniques and they both exist in IEEE 802.11 systems.

Frequency hopping spread spectrum FHSS

In frequency hopping systems, the carrier frequency changes at a given rate, following a given sequence. This sequence is the code of these systems. The receiver must know the same code in order to follow the sequence. In a given burst the transmitted signal is spread to a larger bandwidth by using a different frequency on every hop but the actual transmitted signal within one hop uses in fact a narrow bandwidth. There are still some advantages in frequency hopping systems [San01, pp.72-73]:

- Interference from a fixed narrowband source only affects those packets that are transmitted at the same frequency. Also a frequency hopping system does not interfere with a fixed bandwidth all the time.

- Two frequency hopping systems with overlapping coverage areas only interfere each other when bursts are sent over the same frequency at the same time.

- In multipath environments only some bursts are affected by frequency selective fading. The total received signal can still be received with a low bit error ratio (BER) value if the amount of interference is limited.

The IEEE 802.11 FHSS method divides the ISM band into a series of 1-MHz channels (bandwidth=1 MHz) that starts with centre frequency 2.400 GHz for channel 0. Channel 1 is at 2.401 GHz and so on up to channel 95 at 2.495 GHz. Authorities regulate the use of frequencies in different countries: the major regulatory domains and the available channels are shown in Table 1 [Gas02, p.167].

Table 1 IEEE 802.11 FHSS channels and hop set sizes in different regulatory domains.

Regulatory domain	Allowed channels	Hop set size
US (FCC)	2 to 79 (2.402 – 2.479 GHz)	26
Canada (IC)	2 to 79 (2.402 – 2.479 GHz)	26
Europe * (ETSI)	2 to 79 (2.402 – 2.479 GHz)	26
France	48 to 82 (2.448 – 2.482 GHz)	27
Spain	47 to 73 (2.447 – 2.473 GHz)	35
Japan (MMK)	73 to 95 (2.473 – 2.495 GHz)	23

* excluding France and Spain

IEEE 802.11 defines mathematical functions for deriving the hopping sequence that can be found in clause 14.6.8 of the IEEE 802.11 specification. As an example, hopping sequence 1 for North America and most of Europe begins with the sequence {3, 26, 65, 11, 46, 79, 50, 22, ...}. IEEE 802.11 defines hopping sequences in such a way that different sets are orthogonal so overlapping during a sequence is avoided. Sizes of orthogonal hop sets are

also regulated by authorities and can be found in Table 1. The dwell time per channel may not exceed 0.4 s [ETS01, p.13]. Switching time between frequencies is specified to 224 µs in IEEE 802.11 [IEE99a, p.180]. The main RF parameters of IEEE 802.11 FHSS are shown in Table 2.

Table 2 Main RF parameters of IEEE 802.11 FHSS.

Bandwidth	1 MHz
Channel spacing	1 MHz
Channel switching time	224 µs
Dwell time (min)	2 ms (hop rate 500 hop/second)
Dwell time (max)	400 ms (hop rate 1.25 hop/second)
Effective radiated power (max)	-10 dBW (100 mW) EIRP
Peak power density (max)	-10 dBW / 100 kHz
Nominal bit rate	1 or 2 Mbit/s
Receiver sensitivity (FER ≤ 3%)	-80 dBm (1 Mbit/s); -75 dBm (2 Mbit/s)
Modulation	2-GFSK (1 Mbit/s); 4-GFSK (2 Mbit/s)

Direct sequence spread spectrum DSSS

In direct sequence systems the spectrum is spread by intentionally increasing the modulation rate. The transmitted data bit sequence is combined with a higher-rate bit sequence (called the chip sequence). The result of this combination is a new sequence at the chip rate. Then this chip sequence is used to modulate the carrier in the transmitter (TX). In the receiver (RX), the inverse operation must be conducted in order to receive the original bit sequence. The signal is demodulated, and recombined with the original chip sequence to restore the original data.

Advantages of direct sequence systems compared to narrowband systems are described as follows [San01, p.77]:

- The power density (W / MHz) is much lower because of the larger bandwidth over which the power is spread. This results in a lower probability of interception and lower interference to other systems.
- Privacy of communication is increased if the chip sequence is kept secret.
- In the receiver the data is restored to the original bit rate, which is much smaller than the chip rate. The signal is despread back to the original data signal, and the components lying outside this signal can be filtered out. Any other signal, including noise and interference of all kind, will have a wide bandwidth after combination with the chip sequence and most of their power will be filtered. Note that narrowband interference would be spread

throughout the corresponding chip band after combining with the chip sequence.

In IEEE 802.11 the chip sequence is public so privacy features cannot be applied as such. The reason for using the direct sequence method is its ability to share the spectrum with other users causing low level of interference.

IEEE 802.11 uses an 11-bit Barker word as a pseudorandom noise code. The entire Barker word is used as a chipping sequence to encode each bit. The benefit of using Barker words in IEEE 802.11 is that it offers good autocorrelation properties. This means that the autocorrelation function at RX operates as expected in a wide variety of environments and is relatively tolerant to multipath delay spreads [Gas02, p.179]. The processing gain is equal to 11 (10.4 dB), which allows a small margin of safety compared to the value 10 dB as required by the authorities.

In DSSS the channels used are much wider than in FHSS. There are 14 channels in the 2.4 GHz ISM band each 5 MHz wide. Channel 1 is located at 2.412 GHz, channel 2 at 2.417 GHz and so on up to channel 14 at 2.484 GHz. Table 3 summarises the allowed channels in DSSS in different regulatory domains [Gas02, p.180].

Table 3 IEEE 802.11 DSSS channels in different regulatory domains.

Regulatory domain	Allowed channels
US (FCC)	1 to 11 (2.412 – 2.462 GHz)
Canada (IC)	1 to 11 (2.412 – 2.462 GHz)
Europe * (ETSI)	1 to 13 (2.412 – 2.472 GHz)
France	10 to 13 (2.457 – 2.472 GHz)
Spain	10 to 11 (2.457 – 2.462 GHz)
Japan (MMK)	14 (2.484 GHz)

* excluding France and Spain

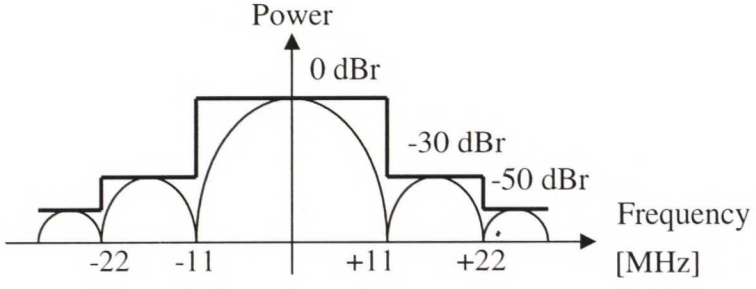

Figure 4 DSSS transmission spectrum mask.

During transmission most of the frequency is spread across a 22 MHz band within a channel. DSSS uses an 11 MHz chip clock and therefore the energy spreads out from the channel centre in multiples of 11 MHz. To prevent

adjacent channel interference there is a transmit spectrum mask specified in IEEE 802.11, which is shown in Figure 4 [IEE99a, p.219]. The first and the second side lobes are filtered to –30 dB and –50 dB below the power at the channel centre, respectively. With 5 MHz channel spacing networks sharing the spectrum must be separated by 5 channels i.e. 25 MHz to prevent overlapping. Therefore only three users within the same network can operate in parallel without overlapping in the available bandwidth. The main RF parameters for IEEE 802.11 DSSS are shown in Table 4.

2.2. IEEE 802.11b

IEEE 802.11b is a physical layer extension to IEEE 802.11 using the same MAC layer. IEEE 802.11b uses also the same channel spacing, effective radiated power and signal bandwidth as IEEE 802.11 and it also operates in the unlicensed 2.4 GHz ISM band. The maximum number of parallel operating systems is also three using the available bandwidth, as in IEEE 802.11. IEEE 802.11b introduces a high-rate direct sequence physical layer (also called HR/DSSS) that is capable of 5.5 Mbit/s and 11 Mbit/s nominal bit rates in addition to 1 Mbit/s and 2 Mbit/s in IEEE 802.11. This is achieved by using another modulation method: complementary code keying (CCK) [IEE99b, p.11]. The receiver sensitivity level and the maximum received signal level have changed, and the correct values for FER $\leq 8x10^{-2}$ using CCK with rate of 11 Mbit/s are -76 dBm and -10 dBm, respectively [IEE99b, p.57].

The data rate is dynamically negotiable and varies depending on various factors, including range (1-2 Mbit/s up to 120 metres (400 feet) and max of 11 Mbit/s up to 45 metres (150 feet) [Gru, p.1]. The main RF parameters for IEEE 802.11b DSSS are also shown in Table 4.

Table 4 Main RF parameters of IEEE 802.11 and 802.11b DSSS.

Bandwidth	22 MHz
Channel spacing	5 MHz
Spreading sequence	11 chip Barker sequence: +1, -1, +1, +1, -1, +1, +1, +1, -1, -1, -1
Processing gain	10.4 dB
Effective radiated power (max)	-10 dBW (100 mW) EIRP (Europe)
Peak power density (max)	-20 dBW / 1 MHz
Nominal bit rate	1, 2, 5.5 or 11 Mbit/s
Receiver sensitivity (FER ≤ 8%)	-80 dBm (2 Mbit/s); -76 dBm (11 Mbit/s)
Max received signal level (FER ≤ 8%)	-4 dBm (2 Mbit/s); -10 dBm (11 Mbit/s)
Modulation	DBPSK (1 Mbit/s); DQPSK (2 Mbit/s) CCK (5.5 and 11 Mbit/s)

2.3. IEEE 802.11g

IEEE 802.11g is another physical layer extension to IEEE 802.11 that operates in the 2.4 GHz ISM band. As its predecessors IEEE 802.11g also specifies three parallel available radio channels. The maximum transfer rate is 54 Mbit/s per channel, which is achieved by using orthogonal frequency division multiplexing (OFDM) modulation [Kee02]. The beauty of IEEE 802.11g is its backward compatibility with 802.11b: 802.11g devices can interoperate with existing 802.11b devices [Gre, p.2]. While writing this thesis the standardisation process of 802.11g has just come to an end.

2.4. Other wireless LAN techniques

There exist various other wireless LAN techniques in addition to those presented in preceding sections. In this section these techniques are mentioned briefly.

The IEEE 802.11 family of standards specifies also other WLAN techniques. IEEE 802.11a uses the U-NII (Unlicensed National Information Infrastructure) radio band at 5 GHz that covers the frequencies 5.15 – 5.35 GHz and 5.725 – 5.825 GHz. The use of IEEE 802.11a is prohibited in Europe. IEEE 802.16 WirelessMAN™ is a metropolitan area network for connecting urban buildings to the backbone network using the frequency range 10 – 66 GHz. IEEE 802.16a is an extension to IEEE 802.16 that extends the frequency range covering also 2 – 11 GHz.

Hiperlan/2 is a standard developed by the European Telecommunications Standards Institute (ETSI) as a replacement of the IEEE 802.11a for Europe. Hiperlan/2 uses the 5 GHz band, covering frequencies 5.150 – 5.350 GHz and 5.470 – 5.725 GHz.

Bluetooth™ and HomeRF are techniques using the 2.4 GHz ISM band. They are both low range RF-systems intended for indoor use but particularly HomeRF can cause interference to other systems since it uses a bandwidth of 5 MHz with the maximum power of 24 dBm.

2.5. RF challenges in 2.4 GHz frequency band

Since the cost of licensing the spectrum for radio transmission is significant, the users have turned attention to unlicensed frequency bands. Unlicensed frequency bands are free to use, authorities are limiting only the radiation power. The 2.4 GHz ISM band is currently the most popular frequency band that is available in many parts of the world [Ho02, p.783]. Because of the popularity, the use of the frequency band has grown rapidly by users and by technologies. Besides WLAN techniques, the 2.4 GHz ISM band is also used by other intentionally radiating systems, such as medical instruments and e.g. in Finland radio amateurs and remote sensing devices [Vie03].

Also unintentional radiators cause interference. The most common unintentional radiator is the microwave oven, which operates in the same band. During the active period the emitted signal is a continuous wave (CW) that spreads to the bandwidth of 2 to 15 MHz for residential ovens and up to tens of MHz for commercials ovens [Ho02, p.783]. A DSSS system with processing gain can tolerate narrowband interference very well. However, performance degradation is significant if the interference covers a large portion of the bandwidth operated by the system.

3. Radio wave propagation

Radio wave propagation plays a significant role in the performance of radio systems. Radio waves, i.e. electromagnetic waves, propagate in a radio channel that is understood as the radio path between the transmitter and the receiver, including antennas. The radio path consists of a variable environment and various obstacles that affect the way the radio waves propagate.

Radio wave propagation could be modelled exactly by using Maxwell's equations for electromagnetic field theory, but this method would be mathematically restrictively complex and is therefore not included in this thesis.

Fixed radio systems (e.g. terrestrial radio relay systems) are planned in such a way that there are no obstacles that cause attenuation in the radio path. This is called line-of-sight (LOS) situation. LOS situation is often impossible to maintain while using mobile radio systems, e.g. WLAN, since these are many times used in an urban environment. In such environments there are usually many objects and reflecting surfaces in the radio path that affect the radio wave propagation. Therefore such a situation is called non-line-of-sight (NLOS).

There are four basic phenomena that are understood as the basic radio wave propagation mechanisms in this thesis: free space loss, reflection and penetration, diffraction, and scattering. They are introduced in Section 3.1.

3.1. Physical propagation mechanisms

The radio path may consist of various obstacles which affect the radio wave propagation. The radio wave can be reflected from the surface of the obstacle and it can penetrate into it. Large obstacles can cause scattering and edges of the obstacles can diffract the signal to various directions. Each of these events attenuates the signal.

3.1.1. Free space loss

The most simple radio wave propagation mechanism is free space propagation. It is assumed that there are no obstacles or reflecting surfaces in the radio path between transmitter and receiver. It is also assumed that antennas are separated so they are not located in the near field of each other. Under these assumptions there is no multipath propagation and the wave is not absorbed. Since there are also no reflections, the received power level can be calculated directly as a function of distance between antennas if the transmitted power is known. The power density within a region with a certain radius is proportional to the area where the power is spread. The transmitted radiation in a certain

direction is described by antenna gain and transmitted power P_{TX}. The power is spread spherically. Thus, at distance r the power density S_d is given by (1) [Lin96, p.8]:

$$S_d = \frac{G_{TX} P_{TX}}{4\pi r^2} \quad (1)$$

The receiving antenna intercepts this power density using a cross section A_e that is defined as a function of antenna gain G_{RX} and wavelength λ, as shown in (2) [Lin96, p.8]:

$$A_e = \frac{\lambda^2}{4\pi} G_{RX} \quad (2)$$

Therefore, the received power can be calculated by using (3) [Lin96, p.8]:

$$P_{RX} = A_e S_d = G_{TX} G_{RX} P_{TX} \left(\frac{\lambda}{4\pi r} \right)^2, \quad (3)$$

where the term $(\lambda/4\pi r)^2$ is the actual free space loss, which is normally denoted as L_0. In many cases the free space loss is given in dB as in (4):

$$L_0 = 32.45 + 20\log f_{[MHz]} + 20\log r_{[km]} \quad (4)$$

3.1.2. Reflection and penetration

When the radio wave hits a surface large enough in comparison with its wavelength, part of its power is reflected from the surface and part of it penetrates through the surface. The dimensions of the reflection surface are defined by a Fresnel's zone that is discussed in Section 3.1.3.

The reflection angle of the radio wave is the same as the incidence angle ϕ_1. The reflection loss depends on the electrical properties of the medium on both sides of the reflecting surface, the frequency used, the incidence angle and the polarization of the radio wave. Figure 5 presents the reflection of both polarisations: perpendicular and parallel [Lin96, p.46]. Parallel polarisation states that magnetic field *H* is parallel to the plane of incidence, whereas perpendicular polarisation states that electric field *E* is parallel to the plane of the incidence. Parallel polarisation is also referred to as vertical polarisation (or TM) and perpendicular polarisation is referred to as horizontal polarisation (or TE).

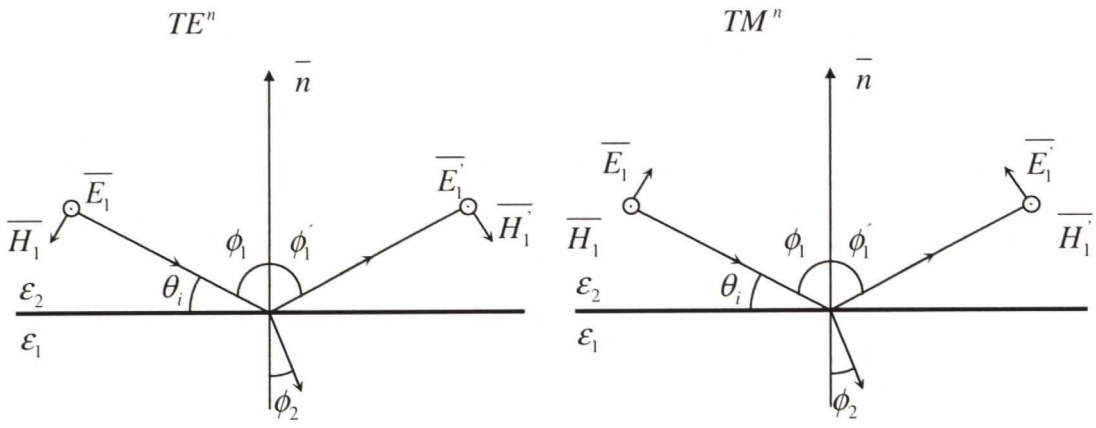

Figure 5 Reflection of perpendicular and parallel-polarised plane wave.

The Fresnel reflection coefficients for perpendicular and parallel polarisation, $\Gamma_\perp$ and $\Gamma_\parallel$, respectively, are presented in (5) and (6) [Lin96, p.47].

$$\Gamma_\perp = \frac{\sin\theta_i - \sqrt{\varepsilon - \cos^2\theta_i}}{\sin\theta_i + \sqrt{\varepsilon - \cos^2\theta_i}} \tag{5}$$

$$\Gamma_\parallel = \frac{\varepsilon\sin\theta_i - \sqrt{\varepsilon - \cos^2\theta_i}}{\varepsilon\sin\theta_i + \sqrt{\varepsilon - \cos^2\theta_i}}, \tag{6}$$

where $\varepsilon = \varepsilon_1/\varepsilon_2$ is the relative permittivity of the materials.

The reflection coefficients depend on the surface of reflection, and equations (5) and (6) are based on the ideal situation. If the surface is spherical or unsmooth there is an additional reduction in the reflection coefficients. In reality the reflections occur usually in urban environments, where the radio wave is reflected from the surface of the earth, walls, cars or other obstacles that are not ideal. Therefore exact modelling of the propagation channel can become very complex.

The part of the radio wave that is not reflected penetrates into inside the surface material. Penetration coefficients for perpendicular and parallel polarisation, $T_\perp$ and $T_\parallel$, respectively, are given in (7) and (8) [Nik92, p.69].

$$T_\perp = 1 + \Gamma_\perp \tag{7}$$

$$T_\parallel = (1 + \Gamma_\parallel)\frac{\cos\phi_1}{\cos\phi_2}, \tag{8}$$

where $\phi_1 = \pi/2 - \gamma$ and ϕ_2 can be calculated using Snell's law (9) [Nik96, p.70]

as a function of incidence angle, permittivity and permeability of the material, $\varepsilon_{1,2}$ and $\mu_{1,2,}$ respectively.

$$\sqrt{\mu_1\varepsilon_1}\sin\varphi_1 = \sqrt{\mu_2\varepsilon_2}\sin\varphi_2 \tag{9}$$

3.1.3. Diffraction

According to Huyghen's principle almost all of the transmitter power propagates within the 1st Fresnel zone. If it is kept clear of obstacles, the radio wave propagates according to the free space propagation principle. If there is an obstacle partly covering the zone, the signal is attenuated. The signal also bends behind the obstacle and this phenomenon is called diffraction. In particular, with diffraction there is still the possibility of receiving the radio signal even without any reflecting surfaces and when there is no line-of-sight between TX and RX.

The radius of the 1st Fresnel zone is calculated with using (10) [Lin96, p.29].

$$b = \sqrt{\frac{\lambda d_1 d_2}{d_1 + d_2}}, \tag{10}$$

where λ is wavelength and $d_{1,2}$ are distances between antenna and obstacle as shown in Figure 6.

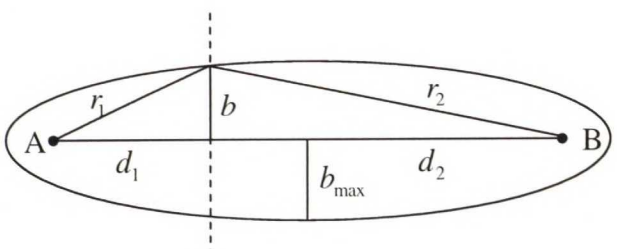

Figure 6 Fresnel zone.

The radius is at maximum, when the obstacle is at the centre of the node, as in (11).

$$\begin{aligned} & d_1 = d_2 = 0.5d \\ & \Rightarrow b_{max} = \frac{\sqrt{\lambda d}}{2} \end{aligned} \tag{11}$$

An obstacle penetrating into the 1st Fresnel zone causes attenuation that can be estimated according to the shape of the obstacle. Knife-edge diffraction (Figure 7) is referred to when the obstacle is assumed to be an indefinitely thin plate. The attenuation can be approximated according to (12) [Lin96, p.36].

$$F \approx 0.452\left(\sqrt{(v-0.1)^2+1}-(v-0.1)\right), \tag{12}$$

where v depends of the height H of the obstacle, as in (13).

$$v = \sqrt{2}\frac{H}{b} \tag{13}$$

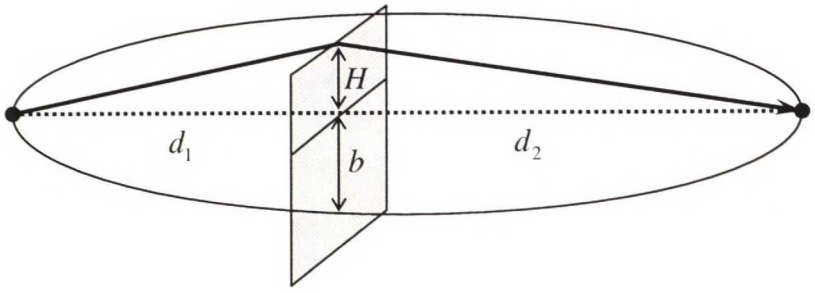

Figure 7 Knife-edge diffraction.

Naturally, all objects that cause diffraction are not sharp. Hills and other rounded objects can cause rounded obstacle diffraction loss that is greater that knife-edge diffraction, and objects that are shaped like wedges or corners cause a different kind of diffraction. These situations are dealt with more thoroughly e.g. in [Lin96] or [Hol00].

3.1.4. Scattering

Scattering propagation is referred to, when an obstacle or particle with dimensions that are small related to the wavelength, alters the radio wave propagation by retransmitting the signal in various directions. If there are a large amount of particles, a substantial amount of transmitter power can be lost. However, scattering can also help transmission by reflecting the radio wave behind shadows or obstacles to positions that are normally out of reach of the radio system. Also, in multipath environments, scattering can strengthen the received signal since new multipath channels are formed by the scattering elements. However, scattering causes polarisation cross coupling and therefore the received signal might not have the same polarisation as the transmitted signal. At high frequencies, atmospheric gases and rain cause scattering losses to signals.

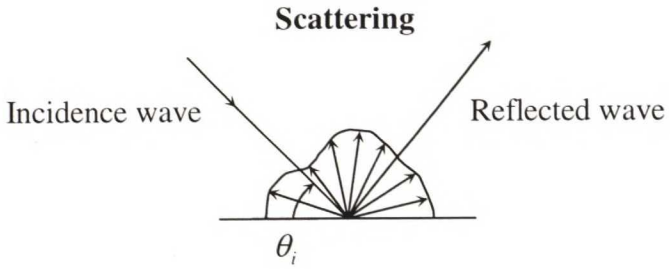

Figure 8 Scattering caused by unsmooth surface.

Reflection from an unsmooth surface causes scattering as shown in Figure 8. The power scattered from an unsmooth surface can be calculated by using (14) [Rap96, p.101][Ame53, p.145]

$$\rho_s = e^{\left[-8\left(\frac{\pi \cdot \sigma_h \cdot \sin\theta_i}{\lambda}\right)^2\right]}, \tag{14}$$

where θ_i is the angle of incidence and σ_h is the standard deviation of the surface height about the mean surface height. It is assumed that the surface height is a Gaussian distributed random variable.

4. Existing channel models

Various radio wave propagation channel models have been developed to estimate the path attenuation, or other parameters of the propagation channel. There are variations in calculation methods, initial values, and results between different models.

Channel models can be categorised in many ways, for instance according to how they are created. Empirical models are based on statistical analysis of a large amount of measurements. Usually the simplest models estimate the path loss with the aid of a set of diagrams that are based on empirical measurements. These models can be scaled to a certain environment using simple parameters such as antenna heights. COST231 Hata-model (European Co-operation in the field of Scientific and Technical Research, action 231) is an example of such a model. It uses frequency, distance between TX and RX, and antenna heights as initial parameters. The environment is also characterised by selecting the environment type from dense city, city, suburban or rural environment.

Semi-deterministic models are more complex and based on theoretical calculations and statistics in addition to empirical measurements. The environmental impacts can be modelled more accurately by adding some theoretical aspect to the models. Therefore, these models require extra parameters to characterise the environment. This leads to the situation where the channel models are more environment-specific and need to be recalculated if the conditions change. COST231 Walfisch-Ikegami model is probably the most familiar semi-deterministic channel model for an urban environment. It uses additional parameters, such as building height, street width, block size and direction of the streets.

Deterministic models are based on electromagnetic simulation of the environments. They try to estimate all the characteristics of the radio channel including delays, polarisations and directions of the multipath components. They are based on 3-dimensional maps of the environment and require heavy calculations in order to model the radio channel thoroughly. Deterministic channel models are environment-dependent, and it is hard (or impossible) to find a model that would suit all environments. Finite difference time-domain (FDTD) methods, used for deriving the impulse response, and Ray-tracing approach, where dominant propagation paths are predicted, are well-known methods to create deterministic channel models.

Radio wave propagation channels can also be divided according to the effects of the channel on the transmitted signal. Traditionally, propagation models have

focused on giving estimations for average received signal strength at a certain distance from the transmitter. These simple models are used to estimate the path loss of the radio channel, and are called large-scale propagation models. On the other hand, propagation models that characterise rapid changes of the signal strength over very short distances (a few wavelengths) between TX and RX or short durations (in the order of seconds), are called small-scale or fading models. Examples of large-scale and small-scale models are presented in Sections 4.1 and 4.2, respectively.

Many channel models deal with different environment and cell types. International Telecommunications Union's (ITU) Recommendation ITU-R P.1411 defines these environments and cell types of radio systems in a suitable way for this thesis. The definitions of different physical operating environments and cell types are shown in Table 5 and Table 6, respectively [ITU03a, pp. 2-3].

Table 5 Physical operating environments.

Environment	Description and propagation impairments of concern
Urban high-rise	Urban canyon, characterized by streets lined with tall buildings of several floors each Building height makes significant contributions from propagation over roof-tops unlikely Rows of tall buildings provide the possibility of long path delays Large numbers of moving vehicles in the area act as reflectors adding Doppler shift to the reflected waves
Urban/suburban low-rise	Typified by wide streets Building heights are generally less than three stories making diffraction over roof-top likely Reflections and shadowing from moving vehicles can sometimes occur Primary effects are long delays and small Doppler shifts
Residential	Single and double storey dwellings Roads are generally two lanes wide with cars parked along sides Heavy to light foliage possible Motor traffic usually light
Rural	Small houses surrounded by large gardens Influence of terrain height (topography) Heavy to light foliage possible Motor traffic sometimes high

Table 6 Definition of cell types.

Cell type	Cell radius	Typical position of base station antenna
Small macrocell	0.5-3 km	Outdoor; mounted above medium roof-top level, some surrounding buildings are above BS
Microcell	100 to 500 m	Outdoor; mounted below medium roof top level
Picocell	Up to 100 m	Indoor or outdoor (mounted below roof-top level)

4.1. Large-scale propagation models

Propagation models that estimate the mean signal strength for different distances between TX and RX in the order of several hundreds or thousands of meters are called large-scale propagation models. Large-scale models are quite simple and do not take in account very small variations e.g. fading caused by multipath propagation. These models are useful e.g. in predicting coverage of a radio system.

Many models that are found in the literature are created for estimating the propagation losses in a macrocell environment using frequencies below 2 GHz. These models can be created for various environments, e.g. COST231 Hata model for rural, suburban and urban environments and COST231 Walfisch-Ikegami model for urban environments. Nevertheless, modern radio systems use higher frequencies or demand higher capacity, and therefore the cell size is decreasing. For instance, outdoor WLAN systems operate above 2 GHz and mainly in microcells. Therefore, efforts have also been directed towards studying microcell propagation above 2 GHz, and channel models can be found especially for city environment e.g. Har-Xia-Bertoni model for microcell city environment [Har99a]. These models take into account the street-guided wave, which is a distinct characteristic of microcells. However, according to Parsons, the models that exist at present are only valid in flat urban areas and the effects of terrain variations or vegetation are largely ignored [Par00, p.108]. Nevertheless, QinetiQ's rather complex generic model for frequencies 1-60 GHz, covers propagation through vegetation [Rog02], which can be used to estimate propagation outside the city environment. Also ITU-R Recommendation P.1546 offers a method for point-to-area predictions for terrestrial services in the frequency range 30 MHz – 3 000 MHz, but it is only valid for the distance range 1 – 1 000 km, which makes it unsuitable for WLAN systems.

Large-scale fading models typically include path loss over distance and shadowing models. In this section, various channel models for various environments are presented, while the emphasis is on models suitable for WLAN usage. Sections 4.1.1 to 4.1.5 consider the path loss channel models, and Section 4.1.6 deals with the shadowing model.

4.1.1. Log-distance path loss model

Theoretical analysis and measurements have indicated that the average received signal power decreases logarithmically over distance in both indoor and outdoor radio channels. The model for average large-scale path loss for arbitrary distances between TX and RX is expressed as a function of distance by using a path loss exponent, n, which indicates the rate at which the path

loss increases with the distance. The log-distance path loss model is shown in (15) [Rap96, p.102].

$$L[dB] = 10 \cdot \log\left(\frac{P_{TX}}{P_{RX}}\right) = L(d_0) + 10 \cdot n \cdot \log\left(\frac{d}{d_0}\right), \quad (15)$$

where d_0 is the reference distance which is determined from measurements and d is the distance between TX and RX. The reference distance should be selected far enough and it should be in the far field of the antenna so that near-field effects do not affect the path loss. Typical reference distance for outdoor microcell systems is 100 meters. Typical path loss exponent values for different environments are shown in Table 7.

Table 7 Path loss exponents for different environments.

Environment	Path loss exponent, n
Free space	2
Urban area cellular radio	2.7 to 3.5
Shadowed urban cellular radio	3 to 5
Obstructed in building	4 to 6
Obstructed in factories	2 to 3

4.1.2. COST231 Hata model

The COST231 Hata model is an empirical model that is based on four parameters: frequency f, distance d, base station antenna height h_{BS} and mobile station antenna height h_{MS}. The Hata model was originally generated for frequencies of 150-1500 MHz for four environments; dense city, city, suburban and rural area. Within the COST231 framework, the model has then been extended the model to frequencies 1500-2000 MHz. The average transmission path loss is given by the following equations [COS99, pp.134-135][Rap96, p.119].

$1) f = 150...1500MHz$

$$\begin{aligned} L &= 69.55 + 26.16\log(f) - 13.82\log(h_{BS}) - a_i(h_{MS}) \\ &+ (44.9 - 6.55\log(h_{BS}))\log(d) \end{aligned} \quad (16)$$

MS-antenna height correction in dense cities:

$$a_1(h_{MS}) = \begin{cases} 8.29(\log(1.54h_{MS}))^2 - 1.1 & \text{for } f \le 300MHz \\ 3.2(\log(11.75h_{MS}))^2 - 4.97 & \text{for } f \ge 300MHz \end{cases} \quad (17)$$

MS-antenna height correction in cities:

$$a_2(h_{MS}) = (1.1\log(f) - 0.7)h_{MS} - (1.56\log(f) - 0.8) \tag{18}$$

MS-antenna height correction in suburban areas:

$$a_3(h_{BS}) = a_2(h_{BS}) + 2\left(\log\left(\frac{f}{28}\right)\right)^2 - 5.4 \tag{19}$$

MS-antenna height correction in rural areas:

$$a_4(h_{MS}) = a_2(h_{MS}) - 4.78(\log(f))^2 - 18.33\log(f) - 40.98 \tag{20}$$

$2)\, f = 1500...2000MHz$

$$\begin{aligned} L &= 46.3 + 33.9\log(f) - 13.8\log(h_{BS}) - a_i(h_{MS}) \\ &+ (44.9 - 6.55\log(h_{BS}))\log(d) + C_m \end{aligned} \tag{21}$$

$$C_m = \begin{cases} 3dB, \text{ in metropolitan centres} \\ 0dB, \text{ elsewhere} \end{cases}$$

The following parameter ranges are allowed:

$$\begin{cases} d : 1...20km \\ h_{BS} : 30...200m \\ h_{MS} : 1...10m \end{cases}$$

4.1.3. COST231 Walfisch-Ikegami model

The COST231 Walfisch-Ikegami (COST231 W-I in this thesis) model gives a more precise path-loss estimation than the COST231 Hata model. This is due to additional data parameters, which describe the characteristics of the environment: building heights h_{roof}, width of the roads w, building separation b and road orientation with respect to the direct radio path φ. The model distinguishes between LOS and NLOS situations. The path losses for both situations are given by the following equations [COS99, pp.136-139].

LOS-case:

$$L = 42.6 + 26\log d_{[km]} + 20\log f_{[MHz]} \tag{22}$$

NLOS-case is composed of the terms of free space loss L_0, roof-to-street diffraction and scatter loss L_{rts}, and multiple screen diffraction loss L_{msd}.

$$L = L_0 + L_{rts} + L_{msd} \tag{23}$$

$$L_0 = 32.5 + 20\log d_{[km]} + 20\log f_{[MHz]} \tag{24}$$

$$L_{rts} = -16.9 - 10\log w_{[m]} + 10\log f_{[MHz]} + 20\log\left(h_{roof} - h_{MS}\right) + L_{ori} \tag{25}$$

L_{ori} takes into account the street orientation:

$$L_{ori} = \begin{cases} -10 + 0.354\varphi, & 0^\circ \le \varphi \le 35^\circ \\ 2.5 + 0.075(\varphi - 35), & 35^\circ \le \varphi \le 55^\circ \\ 4.0 - 0.114(\varphi - 55), & 55^\circ \le \varphi \le 90^\circ \end{cases} \tag{26}$$

Multiple screen diffraction loss L_{msd} is calculated from the heights of buildings and their special separations along the radio path.

$$L_{msd} = L_{bsh} + k_a + k_d \log d_{[km]} + k_f \log f_{[MHz]} - 9\log b_{[m]} \tag{27}$$

$$L_{bsh} = \begin{cases} -18\log\left(1 + h_{BS} - h_{roof}\right), & h_{BS} \ge h_{roof} \\ 0, & h_{BS} \le h_{roof} \end{cases} \tag{28}$$

$$k_a = \begin{cases} 54, & h_{BS} \ge h_{roof} \\ 54 - 0.8\left(h_{BS} - h_{roof}\right), & h_{BS} \le h_{roof}, d \ge 0.5km \\ 54 - 0.8\left(h_{BS} - h_{roof}\right)\dfrac{d_{[km]}}{0.5}, & h_{BS} \le h_{roof}, d \le 0.5km \end{cases} \tag{29}$$

$$k_d = \begin{cases} 18, & h_{BS} \ge h_{roof} \\ 18 - 15\dfrac{h_{BS} - h_{roof}}{h_{roof}}, & h_{BS} \le h_{roof} \end{cases} \tag{30}$$

$$k_f = \begin{cases} -4 + 0.7\left(\dfrac{f_{[MHz]}}{925} - 1\right), & \text{small cities} \\ -4 + 1.5\left(\dfrac{f_{[MHz]}}{925} - 1\right), & \text{large cities} \end{cases} \tag{31}$$

The term k_a represents the increase of the path loss for base station antennas below rooftops of the adjacent buildings. The terms k_d and k_f control the dependence of the multi-screen diffraction loss versus distance and radio frequency, respectively.

The following parameter ranges are allowed:

$$\begin{cases} d: 20m...5km \\ f = 800...2000MHz \\ h_{BS} = 4...50m \\ h_{MS} = 1...3m \end{cases} \qquad \begin{cases} w: 25m \\ h_{roof}: 20m \\ b: 200m \end{cases}$$

The COST231 W-I model is quite accurate for measurements of the base station height above rooftop level. However, the prediction error becomes large when the base station height approaches rooftop level. Furthermore, the performance of the model is poor when the base station heights are below rooftop level [COS99, p.139]. After the publication of the COST231 W-I model, its accuracy to predict the diffraction loss from the last rooftop to the street was questioned. Har states that the model predicts path loss 8.7 dB more optimistically than it is supposed to do. However, this error does not affect the path loss variations according to frequency, street width and building height [Har99b, p.1452].

4.1.4. Attenuation in vegetation (ITU-R P.833)

Attenuation in vegetation is dealt with in ITU-R Recommendation P.833, which provides a simple attenuation model for additional attenuation caused by vegetation in the frequency range 30 MHz – 60 GHz. In short-range outdoor radio communication systems attenuation in vegetation can play a significant role and it is important to take that into consideration. However, the wide range of conditions and types of foliage makes it difficult to develop a generalized prediction procedure. ITU-R P.833 introduces a general model of attenuation which is based on measurements. A more detailed and also more complex model for attenuation in vegetation is introduced in 4.1.5.

Terrestrial path with one terminal in woodland

For a terrestrial radio path where one terminal is located within woodland, the additional loss due to vegetation can be characterised according to (32) [ITU03b, p. 1]:

$$A_{ev} = A_m \left(1 - e^{-\frac{d\gamma}{A_m}} \right), \qquad (32)$$

where d is the length of the path within woodland (m), γ is the specific attenuation for very short vegetative paths (dB/m) and A_m is the maximum attenuation for one terminal within a specific type and depth of vegetation (dB). Figure 9 [ITU03b, p. 2] clarifies the situation. The excess attenuation A_{ev} is defined as excess to all other mechanisms, not just free space loss. Thus if the radio path geometry in Fig. 1 were such that full Fresnel clearance from the terrain did not exist, then A_{ev} would be the attenuation in excess of both free-space and diffraction loss.

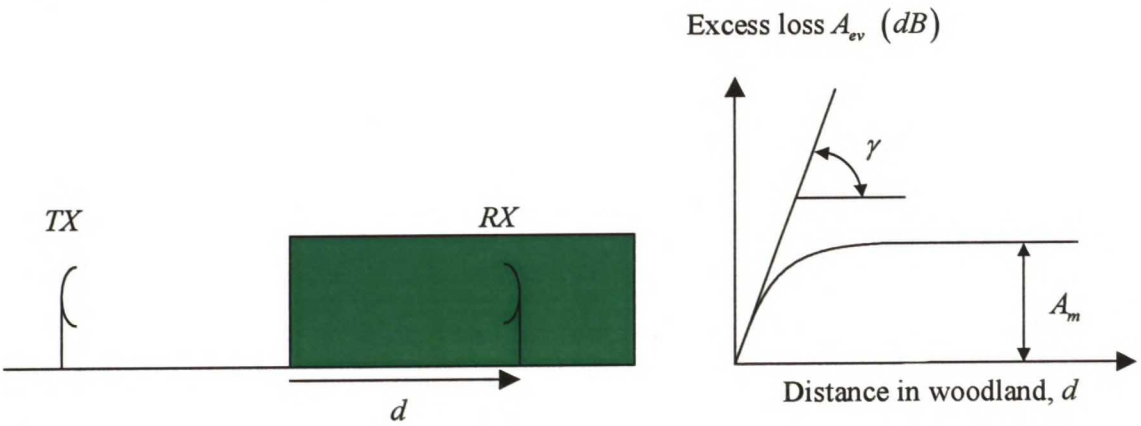

Figure 9 Representative radio path in woodland.

The value of γ depends on the species and density of the vegetation. Figure 10 [ITU03b, p. 3] shows typical values for specific attenuation derived from various measurements over the frequency range 30 MHz to about 30 GHz in woodland. Below about 1 GHz there is a tendency for vertically polarized signals to experience higher attenuation than horizontally, due to scattering from tree-trunks.

The maximum attenuation A_m depends on the species and density of the vegetation, plus the antenna pattern of the terminal within the vegetation and the vertical distance between the antenna and the top of the vegetation.

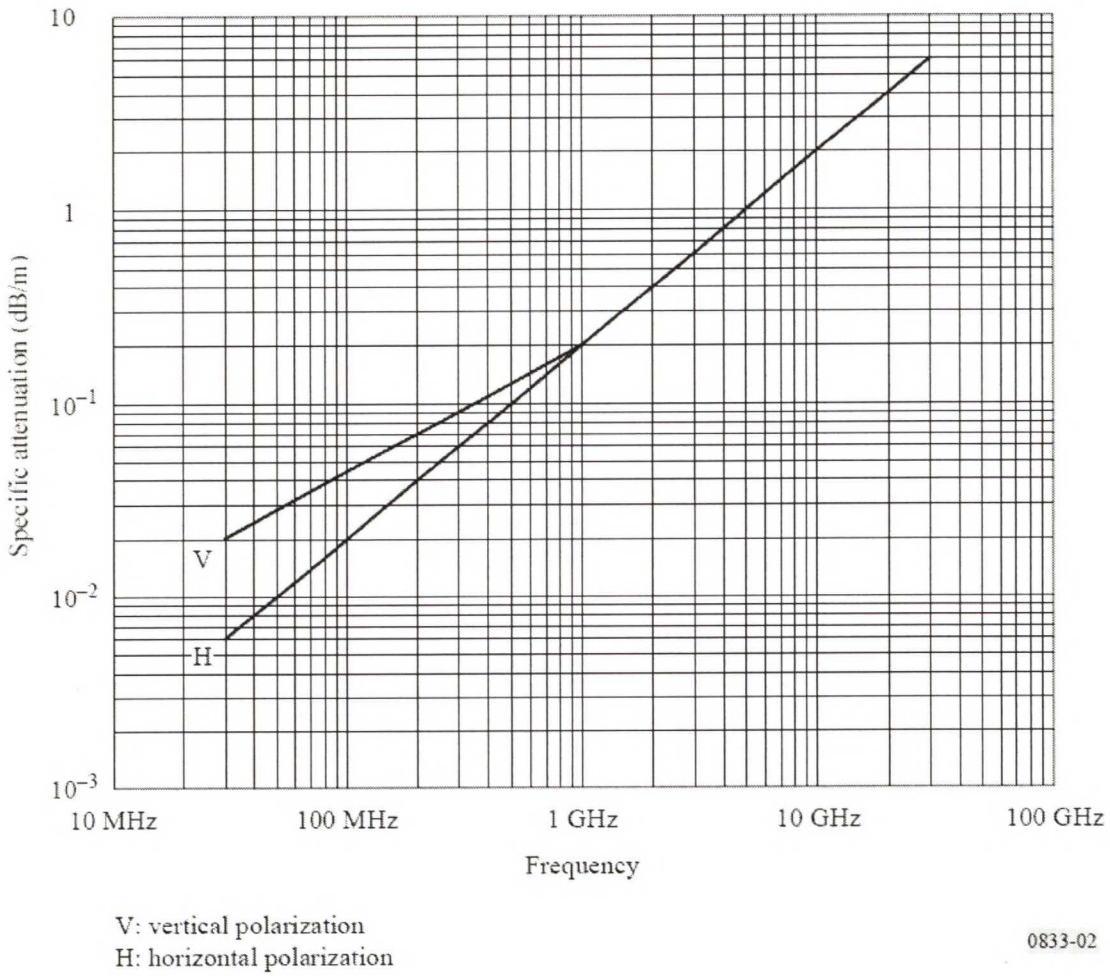

Figure 10 Specific attenuation due to woodland.

The frequency dependent equation of A_m (dB) can be seen in (33) [ITU03b, p. 3].

$$A_m = A_1 f^{\alpha}, \text{ where} \tag{33}$$

f is the frequency (MHz) used, A_1 and α are derived from the measurements:

- Measurements in the frequency range 900-1 800 MHz carried out in a park with tropical trees in Rio de Janeiro (Brazil) with a mean tree height of 15 m have yielded $A_1 = 0.18dB$ and $\alpha = 0.752$. The receiving antenna height was 2.4 m. For example, an interpolation result at 2.4 GHz gives $A_m = 62.69dB$.

- Measurements in the frequency range 900-2 200 MHz carried out in a forest near Mulhouse (France) on paths varying in length from a few hundred metres to 6 km with various species of trees of mean height 15

m have yielded $A_1 = 1.15dB$ and $\alpha = 0.43$. The receiving antenna in woodland was a λ/4 monopole mounted on a vehicle at a height of 1.6 m and the transmitting antenna was a λ/2 dipole at a height of 25 m. The standard deviation of the measurements was 8.7 dB. Seasonal variations of 2 dB at 900 MHz and 8.5 dB at 2 200 MHz were observed. For example, an interpolation result at 2.4 GHz gives $A_m = 32.67dB$.

Single vegetative obstruction

Equation (32) does not apply for a radio path obstructed by a single vegetative obstruction where both terminals are outside the vegetative medium, such as a path passing through the canopy of a single tree. At VHF and UHF, where the specific attenuation has relatively low values, and particularly where the vegetative part of the radio path is relatively short, this situation can be modelled on an approximate basis in terms of the specific attenuation and a maximum limit to the total excess loss as shown in (34) and (35) [ITU03b, p. 4].

$$A_{et} = d\gamma \tag{34}$$

$$A_{et} \leq \text{lowest excess attenuation for other paths (dB)} \tag{35}$$

It is emphasised, that A_{et} is only an approximation. In general it will tend to overestimate the excess loss due to the vegetation.

4.1.5. QinetiQ model for propagation through vegetation

QinetiQ's generic model for radio propagation through vegetation for 1-60 GHz can be considered as a quasi-3D-model, as it is based on empirical measurements and deterministic modelling. It resembles deterministic models as it estimates different propagation paths. The model combines edge-diffraction, ground-reflection and a direct (through vegetation) signal, which is modelled using Radiative Energy Transfer (RET). RET is used to predict the attenuation vs. foliage depth using parameters to describe the absorption and scatter cross-section, reflectance, and scatter function of the vegetation. The individual estimated propagation modes that are combined are around, through and underneath the vegetation are shown in Figure 11 [Rog02, p.5].

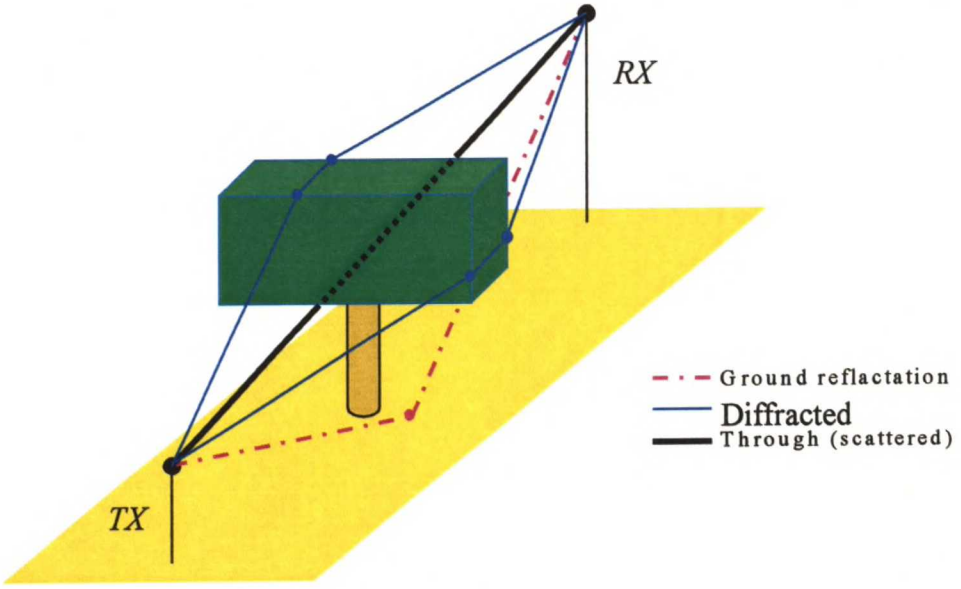

Figure 11 Three modes of propagation; through, around and underneath the vegetation.

The model is suited to micro- and picocells and it is also appropriate for macrocells with the help of some additional databases. The model is based on measurements made at twelve locations in England in 2001-2002. The model is suitable for modelling the propagation through a single tree or multiple trees, in which case the foliage of all trees is modelled in the same way as shown in Figure 11.

Top-diffracted component

The diffraction loss L_{top}, experienced by the signal path over the vegetation can be calculated as double isolated knife-edge diffraction. Figure 12 illustrates the geometry of the top-diffracted component. The component is calculated by using (36) [Rog02, p.33], which is also in accordance with ITU-R Recommendation 526-3.

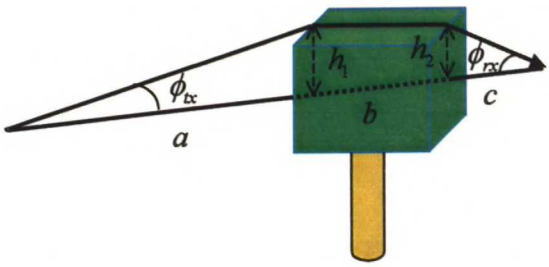

Figure 12 Geometry of top diffracted component.

$$L_{top} = 6.9 + 20\log\left(\sqrt{\left(v(h_1) - 0.1\right)^2 + 1} + v(h_1) - 0.1\right) + G_{TX}(\phi_{tx}) + 6.9 + 20\log\left(\sqrt{\left(v(h_2) - 0.1\right)^2 + 1} + v(h_2) - 0.1\right) + L_c + G_{RX}(\phi_{rx}) \quad (36)$$

where $G_{TX}(\phi_{tx})$ and $G_{RX}(\phi_{rx})$ are the losses due to angles of the diffracted wave from TX antenna and to RX antenna, respectively. L_c is a correction term, shown in (37) [ITU03c, p.15].

$$L_c = 10\log\left[\frac{(a+b)(b+c)}{b(a+b+c)}\right] \tag{37}$$

Side-diffracted component

The diffraction losses L_{sidea} and L_{sideb} are experienced by the signal diffracted around the vegetation. Figure 13 illustrates the geometry of the side-diffracted component.

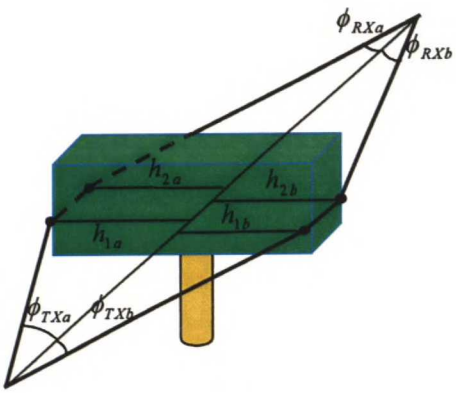

Figure 13 Geometry of side-diffracted component.

Side diffracted component is analogous to top diffracted component and it can be calculated also using (36).

Ground-reflected component

Regarding the ground-reflected component, it is assumed that the path is relatively short so that the geometry shown in Figure 14 applies.

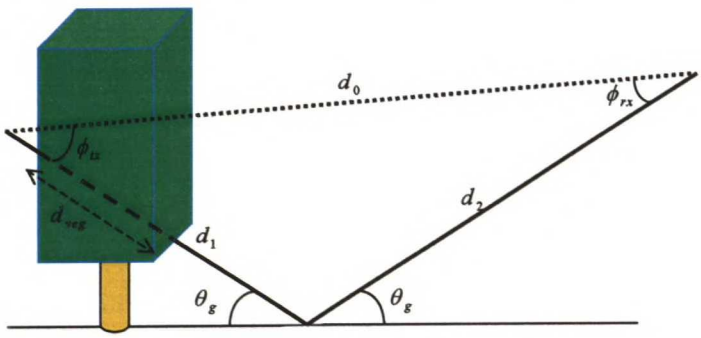

Figure 14 Geometry of ground reflected wave.

To calculate the loss L_{ground} experienced by the ground-reflecting wave, some additional parameters are needed. The ground reflection coefficient R_0 may be calculated using the method presented in Section 3.1.2, with grazing angle θ_g. The values for permittivity and conductance are obtained from ITU-R Recommendation 527-3. The loss of the ground-reflected component can be calculated using (38).

$$L_{ground} = L_{gveg}\left(d_{veg}\right) + 20\log\left(\frac{d_1 + d_2}{d_0}\right), \\ -20\log\left(R_0\right) + G_{TX}\left(\phi_{tx}\right) + G_{RX}\left(\phi_{rx}\right) \tag{38}$$

where $G_{TX}\left(\phi_{tx}\right)$ and $G_{RX}\left(\phi_{rx}\right)$ are the losses due to angles of the diffracted wave from TX antenna and to RX antenna, respectively. $L_{gveg}\left(d_{veg}\right)$ is the loss due propagation of the ground reflected wave through the total vegetation depth d_{veg}. This is calculated in the same way as the through vegetation loss, which is presented next.

Through vegetation or scattered component

The component that propagates through the vegetation is often called scattering component. Following parameters are used to characterise the environment in order to make accurate predictions of the excess attenuation due to vegetation. These parameters are also needed for calculating the loss term.

- α, the ratio of forward scattered power to the total scattered power
- β, the beamwidth of the phase function
- σ_τ, the combined absorption and scatter coefficient
- W, the reflectance (or albedo)
- $\Delta\gamma_R$, the beamwidth of the receiving antenna
- d, the distance into the vegetation in metres

With given frequency, the typical leaf size of the vegetation can be modelled. Additionally, with Leaf Area Index (LAI), the nearest value of preceding parameters can be obtained from the RET tables shown in Table 8 [Rog02, pp.36-37].

Table 8 Fitted values of α , β, W and σ_τ for different species at a frequency of 2 GHz.

	Horse Chestnut *Aesculus hippocastanum L.*	**Silver Maple** *Acer saccharinum L.*	**London Plane** *Platanus hispanica Muenchh*	**Common Lime** *Tilia x europaea*	**Sycamrore** *Acer pseudoplatanus L.*
	In Leaf	Out of Leaf	In Leaf	Out of Leaf	Out of Leaf
LAI			1.93		0.483
Leaf Size	0.300	0.15	0.250	0.100	0.15
α	0.75	0.95	0.95	0.95	0.95
β	80	31	49	60	62
W	0.55	0.95	0.95	0.95	0.95
σ_τ	0.091	0.176	0.203	0.692	0.249

These parameters together with frequency and $\Delta\gamma_{3dB}$, the 3 dB beamwidth of the receive antenna are then used together with the (39).

$$L_{scat} = -10\log\left(\frac{P_R}{P_{max}}\right), \tag{39}$$

where $P_R/P_{\max}$ is given by the RET equation (40).

$$\begin{aligned}
&\frac{P_R}{P_{\max}} = e^{-\tau} && (I_{ri}) \\
&+\frac{\Delta\gamma_R^2}{4}\left(\left(e^{-\hat{\tau}} - e^{-\tau}\right)\bar{q}_M \right. \\
&\left. +e^{-\tau}\sum_{m=1}^{M}\frac{1}{m!}(\alpha W\tau)^m\left(\bar{q}_m - \bar{q}_M\right)\right) && \Big\}(I_1), \\
&+\frac{\Delta\gamma_R^2}{4}\left(-e^{-\hat{\tau}}\frac{1}{P_N} + \sum_{k=\frac{N+1}{2}}^{N}\left(A_k e^{-\frac{\hat{\tau}}{s_k}}\sum_{n=0}^{N}\frac{1}{1-\frac{\mu_n}{s_k}}\right)\right) && (I_2)
\end{aligned} \tag{40}$$

where P_R is the power received by the receiving antenna with a certain gain pattern and $P_{\max}$ is the received signal strength without the vegetation, $m > 10$ and $11 < N < 21$. The following relations also apply:

$$\tau = \sigma_\tau d$$

τ defines the optical density.

$$\bar{q}_m = \frac{4}{\Delta\gamma_R^2 + m\beta^2}$$

$$\mu_n = -\cos\left(\frac{n\pi}{N}\right)$$

$$P_n = \sin^2\left(\frac{\pi}{2N}\right) \qquad \text{for } n = 0, N$$

$$P_n = \sin\left(\frac{\pi}{N}\right)\sin\left(\frac{n\pi}{N}\right) \qquad \text{for } n = 1, 2, ..., N-1$$

$$\hat{\tau} = (1-\alpha W)\tau$$

$$\hat{W} = \frac{(1-\alpha)W}{1-\alpha W}$$

$\hat{W}$ is referred to as reduced reflectance.

The first line of (40) represents I_{ri}, which is usually referred to as the first term, whereas the sum of the second and third line gives I_1, referred to as the second term. These appear in explicit form. The fourth line represents the third term I_2 of the RET equation, which contains the attenuation coefficients s_k and the amplitude factors A_k. These need to be determined numerically using the following expressions:

The attenuation coefficients s_k are determined by the characteristic equation:

$$\frac{\hat{W}}{2}\sum_{n=0}^{N}\frac{P_n}{1-\frac{\mu_n}{s_k}} = 1$$

Values of s_k represent the roots of this equation. There are $N+1$ roots, for which the following applies:

$$S_{0,\ldots,\frac{N}{2}} = -S_{N,\ldots,\frac{N+1}{2}}$$

The amplitude factors A_k are determined by a system of linear equations given by:

$$\sum_{k=\frac{N+1}{2}}^{N}\frac{A_k}{1-\frac{\mu_n}{s_k}} = \frac{\delta_n}{P_N} \quad \text{for} \quad n = \frac{N+1}{2}...N$$

The linear system of equations can be written in matrix form $A \cdot B = C$:

$$\begin{bmatrix} A_{\frac{N+1}{2}} \\ \vdots \\ A_N \end{bmatrix} \cdot \begin{bmatrix} b_{\frac{N+2}{2},\frac{N+2}{2}} & \cdots & b_{\frac{N+2}{2},N} \\ \vdots & & \vdots \\ b_{N,\frac{N+2}{2}} & \cdots & b_{N,N} \end{bmatrix} = \frac{\delta_n}{P_N},$$

where

$$b_{n,k} = \frac{1}{1+\frac{\mu_n}{s_k}} \qquad \text{with} \quad k,n = \frac{N+1}{2}...N$$

$$\delta_n = \begin{cases} 0 \text{ for } n \neq N \\ 1 \text{ for } n = N \end{cases}$$

This system of equations can be solved for A_k using for example Gaussian elimination. The relation between Gaussian pattern antenna beamwidth and 3 dB beamwidth is given by:

$$\Delta\gamma_R = 0.6\Delta\gamma_{3dB}$$

Combination of the individual components

The total loss experienced by a signal propagating through single or multiple trees is then given by the combination of loss terms, as shown in (41).

$$L_{total} = -10\log\left(10^{-\frac{L_{sidea}}{10}} + 10^{-\frac{L_{sideb}}{10}} + 10^{-\frac{L_{top}}{10}} + 10^{-\frac{L_{ground}}{10}} + 10^{-\frac{L_{scat}}{10}}\right) \qquad (41)$$

4.1.6. Log-normal shadowing

The log-distance path loss model presented in Section 4.1.1 does not take into account the fact that there can be significant differences between the radio wave propagation channels of two locations that still have the same distance between TX and RX. This leads to the feature that measured signals are different than the average value given by (15). The difference between these measurements and given equation is random and log-normally distributed about the mean distant-dependent value, as shown in (42).

$$L[dB] = 10 \cdot \log\left(\frac{P_{TX}}{P_{RX}}\right) = L(d_0) + 10 \cdot n \cdot \log\left(\frac{d}{d_0}\right) + X_\sigma \qquad (42)$$

X_σ is a zero-mean Gaussian distributed random variable (in dB), that describes the shadowing with a standard deviation σ (in dB).

4.2. Small-scale propagation models and multipath

Small-scale fading, or simply just fading, describes the rapid changes of the amplitude of radio waves over a short period of time or travelled distance. Multipath fading is caused by interference between multiple receptions of the same signal. The signal travels along different paths, and therefore is received at slightly different times. These multipath components combine at the receiver antenna to give a resulting signal that varies widely in amplitude, phase or polarisation. A common multipath environment is a city, where the multipath components can reflect, penetrate, diffract and scatter from various obstacles and surfaces as shown in Figure 15.

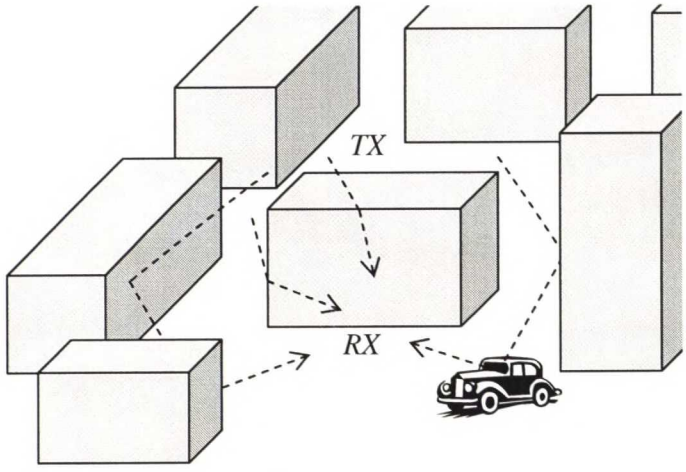

Figure 15 Multipath propagation in city environment.

Many methods have been developed to decrease the effect of multipath propagation. Usage of different diversity methods, e.g. space, time, frequency diversity etc., is a powerful method for reducing multipath fading. Multipath diversity means that multipath components are received in many different ways at the same time to increase the probability of receiving a strong signal at least in one way. For combining the received components, certain techniques, e.g. selection, equal-gain or maximum-ratio combining have been developed. More information about diversity can be found e.g. in [Rap96, p.325]. The RAKE receiver is also a commonly used countermeasure against the adverse effects of multipath propagation in spread spectrum systems like UMTS and WLAN. The RAKE receiver resolves the multipath structure of the channel using estimation, and equals the path delays. Then it performs combining of the signal components e.g. using maximum ratio combining. Also the uses of equalisers or smart antennas are powerful countermeasures against multipath fading.

In general, small-scale propagation channels are time and environment specific. These models require heavy measurement campaigns and the results are correct only for a given measurement location at the measurement instant. These channel models can be divided into narrowband and wideband channel models. Narrowband models are simpler and their behaviour can be modelled with Rayleigh or Rice distribution functions. As the bandwidth increases a tapped delay line model is used with the individual tap amplitudes modelled with independent Rayleigh or Rice distributions. In very wideband channels new statistics of tap amplitude distribution are needed since Rayleigh and Rice distributions give poor models because of insufficient number of components. Measurement results for channels suitable for WLAN systems can be found e.g. in publications [Woo99], [Hea00] or [Vuo01].

4.2.1. Multipath propagation

The three most important effects of small-scale fading caused by multipath propagation and moving scatters are [Rap96, p.139]:

- rapid changes in signal strength over a small travelled distance or time interval,
- random frequency modulation due to varying Doppler shifts on different multipath signals, and
- time dispersion (echoes) caused by multipath propagation delays.

In city environments mobile radio system antenna heights are commonly well below the rooftop level of the surrounding buildings and therefore there might not be a line-of-sight path between TX and RX. Even if a LOS situation occurs there are many reflecting surfaces that still produce multipath components. Relative motion between TX and RX (or surrounding objects causing e.g. reflection) causes random frequency modulation, since each multipath component has a different Doppler shift. The Doppler shift can be calculated by using (43).

$$f_d = \frac{V}{\lambda}\cos\alpha, \tag{43}$$

where V is the velocity of the terminal, α is the spatial angle between the direction of motion of the terminal and the direction of arrival of the wave, and λ is the wavelength.

4.2.2. System functions of the linear time-variant channel

The radio propagation channel can be visualised by a system element that transforms input the signal into an output signal. It is therefore similar to a linear filter with the extension that the radio propagation channel is time-variant. The

radio channel can be modelled as a linear time-variant (LTV) channel that can be characterised by four functions, the time-variant impulse response (also known as the channel delay spread function [Bel63]), the time-variant transfer function, the channel output Doppler-spread function, and the delay/Doppler-spread function.

System functions of the deterministic LTV-channel

The time-variant impulse response $h(\tau,t)$ is shown in (44) [Par00, p.168].

$$h(\tau,t)=\sum_{n=1}^{N} h_n(t)\delta(\tau-\tau_n(t)), \tag{44}$$

where $\tau_n(t)$ is the propagation delay of the nth propagation path as function of time and

$$h_n(t)=\alpha_n(t)e^{-j2\pi f_c\tau_n(t)}, \tag{45}$$

where $\alpha_n(t)$ is the gain of the nth propagation path as function of time and f_c is the carrier frequency.

The time-variant transfer function is obtained by Fourier-transforming the impulse response with respect to the delay variable τ as shown in (46).

$$H(f,t)=F_\tau\{h(\tau,t)\}=\int_{-\infty}^{\infty} h(\tau,t)e^{-j2\pi f\tau}d\tau \tag{46}$$

The output Doppler-spread function is obtained by Fourier-transforming the time-variant transfer function with respect to the time variable t as shown in (47). It describes the channel frequency response to the frequency $f+v$.

$$D(f,v)=F_t\{H(f,t)\}=\int_{-\infty}^{\infty} H(f,t)e^{-j2\pi vt}dt \tag{47}$$

The delay/Doppler-spread function is obtained by Fourier-transforming the time-variant impulse response with respect to the time variable t as shown in (48), or by taking the inverse Fourier-transform of the output Doppler-spread function with respect to frequency. The delay/Doppler-spread function describes the complex gain of the channel in the delay interval $[\tau+d\tau]$ and the Doppler-shift interval $[v+dv]$.

$$S(\tau,\nu)=F_t\{h(\tau,t)\}=\int_{-\infty}^{\infty}h(\tau,t)e^{-j2\pi\nu t}dt \qquad (48)$$

Figure 16 describes the relationships between the system functions. The relationships between system functions are assumed to be deterministic.

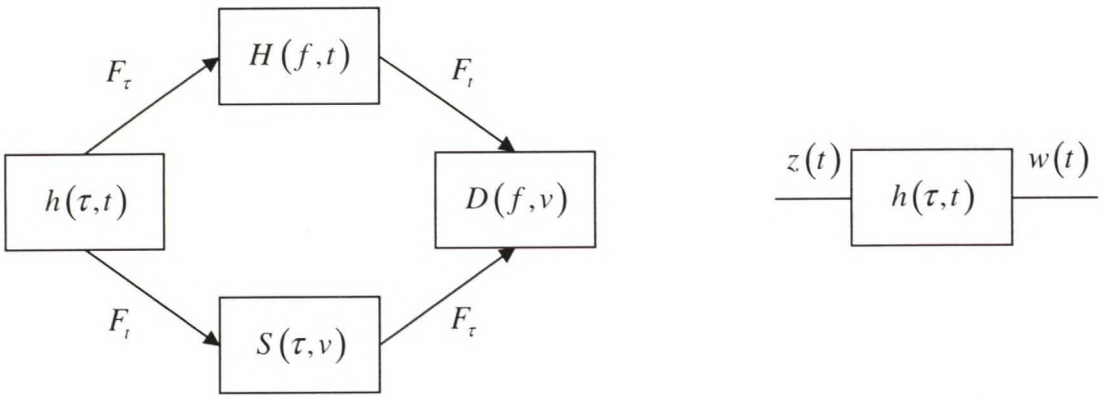

Figure 16 Relationships between deterministic system functions of an LTV-channel.

The characterisation of the system functions can then be extended to practical channels that are randomly time-variant. Wide-sense stationary uncorrelated scattering (WSSUS) channels are an important class of practical channels. More information of LTV-channels can be found e.g. in [Par00, pp.164-190] or in [Bel63].

System functions of the WSSUS random LTV-channel

A randomly time-variant LTV-channel is described using 4-dimensional autocorrelation functions that correspond to the previously described system functions. The use of these 4-dimensional autocorrelation functions is rather unpractical; two assumptions are made in order to get 2-dimensional autocorrelation functions [Pro95, p. 762]

- The LTV-channel under consideration is wide-sense stationary.
- The LTV-channel under consideration is a multipath channel where the propagation paths are statistically independent or at least uncorrelated.

This LTV-channel is called a WSSUS-channel (Wide-Sense Stationary Uncorrelated Scattering). The autocorrelation functions for a WSSUS-channel can be presented as $P_h(\tau,\Delta t), P_H(\Delta f,\Delta t), P_D(\Delta f,\nu)$ and $P_S(\tau,\nu)$ similarly as the previous system functions. The relationships between the autocorrelation functions are presented in Figure 17.

By putting one of the variables to zero, the following one-dimensional functions are obtained [Pro95, pp. 762-766]:

- The multipath intensity profile, also called power delay profile $P_h(\tau,0)$
- The frequency correlation function $P_H(\Delta f,0)$
- The time correlation function $P_H(0,\Delta t)$
- The Doppler power spectrum $P_D(0,\nu)$

Through these functions the characteristic parameters of the WSSUS channel, i.e. delay spread T_m, coherence bandwidth B_m, coherence time T_D, and Doppler-spread B_D, can be obtained.

These multipath channel parameters are useful in order to compare different multipath channels. Delay spread quantifies the time dispersive properties of the channel, coherence bandwidth characterises the channel in frequency domain and Doppler Spread and coherence time describe the time varying nature of the channel.

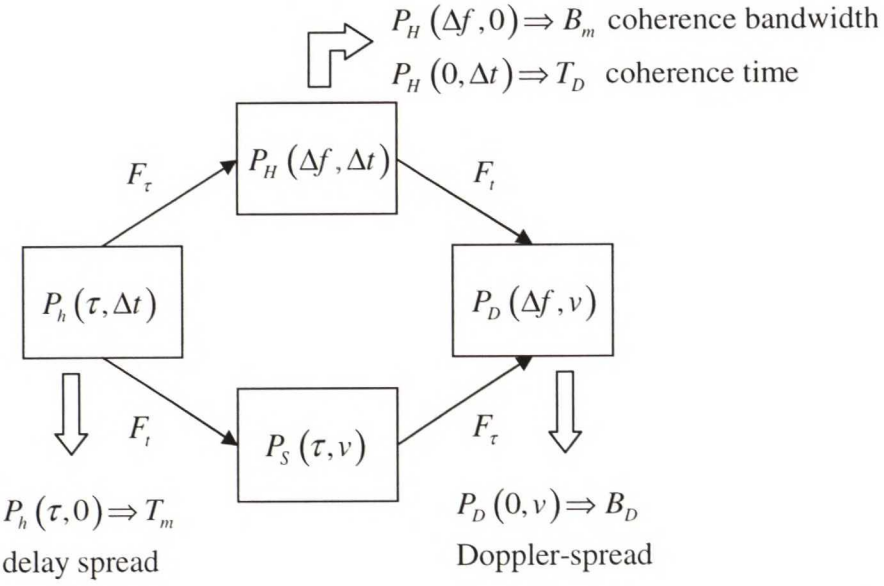

Figure 17 Relationships between autocorrelation functions of a WSSUS channel.

The RMS (root mean square) delay spread S is the square root of the second central moment of the power delay profile (PDP) $P_h(\tau,0)$ as shown in (49) [Par00, p.186].

$$S = \sqrt{\frac{\int_0^\infty (\tau - D)^2 P_h(\tau) d\tau}{\int_0^\infty P_h(\tau) d\tau}}, \tag{49}$$

where D is the mean excess delay of the channel. It is the first moment of the power delay profile (PDP) as shown in (50) [Par00, p.186].

$$D = \sqrt{\frac{\int_0^\infty \tau P_h(\tau) d\tau}{\int_0^\infty P_h(\tau) d\tau}} \tag{50}$$

The coherence bandwidth is a statistical measure of the range of frequencies over which the channel can be considered flat. It is defined as a range of frequencies over which two different frequency components have a strong possibility of amplitude correlation.

The Doppler spread B_D is a measure of the spectral broadening caused by the time rate of change of the mobile radio channel. It is defined as the range of frequencies over which the received Doppler spectrum is essentially non-zero. If the baseband signal bandwidth is much greater than B_D, the effects of the Doppler spread are negligible at the receiver.

The coherence time T_D is the time domain dual of Doppler spread. It is used to characterise the time varying nature of the frequency dispersion of the channel in the time domain. The coherence time is actually a statistic measure of the time domain over which the channel impulse response is essentially invariant. The definition of coherence time implies that the channel affects differently to two signals arriving with a time separation greater than T_D.

4.2.3. Types of small-scale fading

The type of fading depends on the nature of the transmitted signal with respect to the characteristics of the channel. The time dispersion and the frequency dispersion of the channel leads to four different types of fading that depend on the transmitted signal, the channel, and the velocity. While multipath delay spread leads to time dispersion and frequency selective fading, Doppler spread leads to frequency dispersion and time selective fading. The four types of fading are shown in Figure 18 [Rap96, p.166].

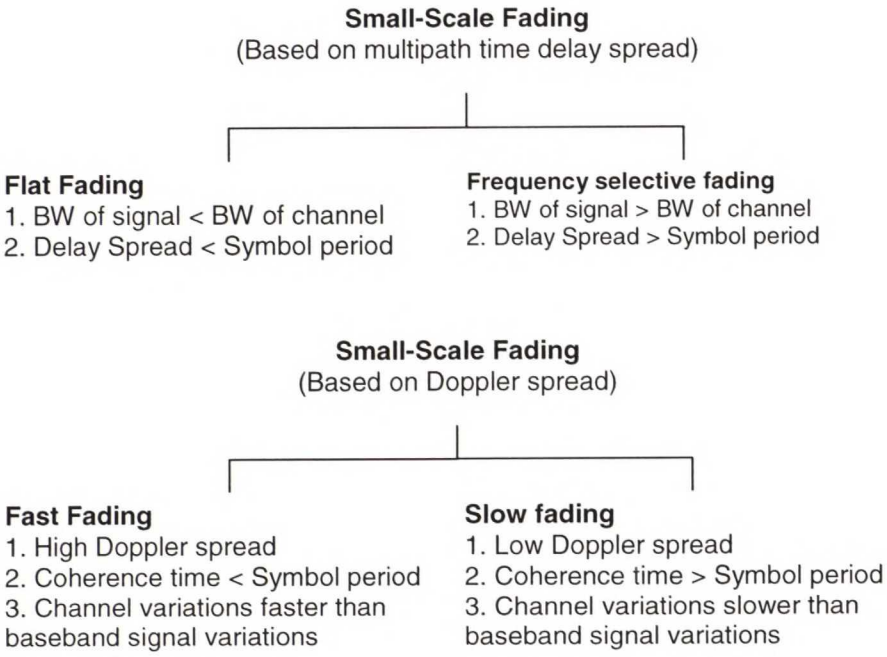

Figure 18 Types of small-scale fading.

Flat fading

The radio channel with constant gain and linear phase response over a bandwidth which is greater than the bandwidth of the transmitted signal, is called flat fading channel. In other words, flat fading occurs when the bandwidth of the transmitted signal is smaller than the coherence bandwidth of the channel, i.e. $B << B_m$. In such a channel, the effect can be seen as decrease of SNR (signal-to-noise ratio). Flat fading channels are also called amplitude varying channels or narrowband channels, since the bandwidth of the applied signal is narrow compared to the bandwidth of the flat fading channel.

Frequency selective fading

The radio channel with constant gain and linear phase response over a bandwidth which is smaller than the bandwidth of the transmitted signal, creates frequency selective fading in the channel. In other words, frequency fading

occurs when the bandwidth of the transmitted signal is greater than the coherence bandwidth of the channel, i.e. $B >> B_m$. This means that different frequency components experience different kinds of attenuation and phase shifts in the channel and therefore can have different gains. Frequency selective fading also causes intersymbol interference (ISI). For frequency selective fading, the spectrum of the transmitted signal has a wider bandwidth than the coherence bandwidth of the channel. This type of fading can be caused by any delay difference between components and the fading increases as the delay spread increases. Frequency selective fading channels are also called wideband channels.

Fast fading

Fast fading occurs if the channel impulse response changes rapidly within the symbol duration. In other words, fast fading occurs when the coherence time of the channel is smaller than the symbol period of the transmitted signal, i.e. $T_D << T$. This causes frequency dispersion (also called time selective fading) due to Doppler spreading. Fast fading (as well as slow fading), deals with the rate of change of the channel due to motion.

Slow fading

Slow fading occurs when the channel impulse response changes at a rate much slower than the transmitted baseband signal. In other words, slow fading occurs when the coherence time of the channel is greater than the symbol period of the transmitted signal, i.e. $T_D >> T$. This means that the channel may be assumed static over one or several reciprocal bandwidth intervals. In the frequency domain the Doppler spread of the channel is much less than the bandwidth of the baseband signal.

The product of the delay spread and Doppler-spread $T_m B_D$ is called the spread factor of the channel. If $T_m B_D < 1$ the channel is said to be underspread; otherwise, it is overspread. For underspread channel it is possible to select the transmitted signal such that these channels are flat fading and slow fading [Pro95, p.771].

4.2.4. Distribution functions

In Section 4.1.6 the log-normal distribution was used to describe the large-scale shadow fading. For small-scale multipath components, the probability density function (PDF) is described by different statistical distribution functions. Rayleigh and Rice distributions can describe the PDF of the signal envelope

changes in multipath situations with assumptions that the channel is flat fading and slow fading [Pro95, pp.772-773].

The Rayleigh distribution is commonly used to describe the statistical time varying nature of the received envelope of a flat fading signal, or the envelope of an individual multipath component [Rap96, p.172]. It is well known that the envelope of the sum of two quadrature Gaussian noise signals obeys the Rayleigh distribution. The PDF of the Rayleigh distribution is given by (51) [Rap96, p.172].

$$p(r)=\frac{r}{\sigma^2}e^{-\frac{r^2}{2\sigma^2}}, \qquad (0\le r\le\infty) \qquad (51)$$

where σ^2 is the time-average power of the received signal before envelope detection, r is the Rayleigh fading signal envelope and $r^2/2$ is the instantaneous power.

In situations when a dominant stationary (nonfading) signal component, such as the line-of-sight component, exists in the channel, the small-scale fading envelope distribution is Ricean. The PDF of the Rice distribution is given by (52) [Rap96, p.176].

$$p(r)=\frac{r}{\sigma^2}e^{-\frac{(r^2+A^2)}{2\sigma^2}}I_0\left(\frac{Ar}{\sigma^2}\right), \qquad (A\ge 0, r\ge 0) \qquad (52)$$

where A is the dominant component of the signal and I_0 is the modified Bessel function of the first kind and zero order.

The Ricean distribution is often described by a parameter K, which is defined as the ratio between the deterministic signal power and the variance of the multipath, as shown in (53). K is called the Ricean factor.

$$K[dB]=10\log\left(\frac{A^2}{2\sigma^2}\right) \qquad (53)$$

When this dominant component exists ($A>0$) the Ricean distribution is generated; whereas when the dominant component fades away (A approaches zero) the Ricean distribution degenerates to the Rayleigh distribution.

4.2.5. Tapped delay line channel model

As earlier mentioned, the Rayleigh and Rice distributions are not suitable for modelling the behaviour of a channel when the bandwidth of the channel

increases. When a bandwidth $W >> B_m$ is available to the user, the wideband channel is generally characterised by the tapped delay line channel model. The channel is still assumed to be slowly fading, i.e. $T << T_D$. For a fixed number of taps, parameters characterising the multipath behaviour, such as excess delay, normalised amplitudes and amplitude distributions, are calculated. The tapped delay line channel is represented by a time-variant FIR-filter in complex equivalent low-pass (ELP) signal domain. The tapped delay line model with K tap coefficients $h_k(t)$, $k = 0,1,...,K-1$ is shown in Figure 19 [Pro95, p.797].

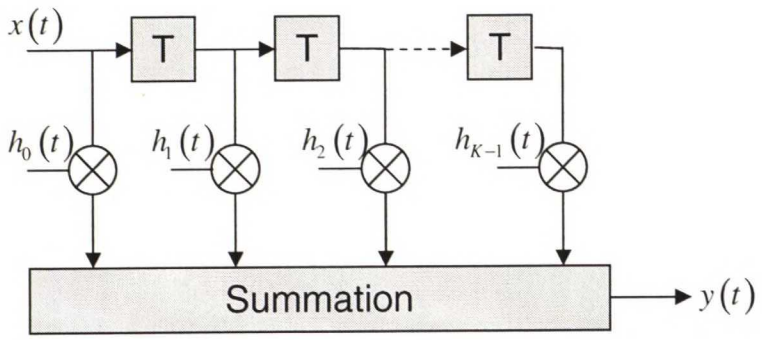

Figure 19 Tapped delay line presentation of a wideband multipath radio channel.

The channel input and output functions, $x(t)$ and $y(t)$ respectively, are generally complex. The unit tap delay of the model is denoted by T, which is an integer multiple of the simulation system sampling interval T_S, usually $T = T_S$ [Rut97, p.303], or $T = 1/W$ [Pro95, p.797], where W is the bandwidth occupied by the real bandpass signal.

Since the total multipath spread is T_m, for all purposes the tapped delay line model for the channel can be truncated at K taps according to (54) [Pro95, p.797].

$$K = (T_m W) + 1 \tag{54}$$

The output function is given by (55).

$$y(t) = \sum_{k=1}^{K} x\left(t - \frac{k}{W}\right) h_k(t), \tag{55}$$

The time-variant tap coefficients $h_k(t)$ are complex-valued stationary random processes. Since $h_k(t)$ represent the tap weights corresponding to the K different delays $\tau = k/W$, $k = 0,1,2,...,K-1$, the uncorrelated scattering

assumption made in Section 4.2.2 implies that $h_k(t)$ are mutually uncorrelated [Pro95, p.797].

The tapped delay line model with only one tap represents the narrowband channel case, and as the bandwidth of the transmitted signal increases the number of taps increases also. In the special case of Rayleigh fading, the magnitudes of the taps are Rayleigh distributed and the phases are uniformly distributed [Pro95, p.797]. However, as the bandwidth increases even more, the Rayleigh or the Rice distributions are no longer valid. In such a case also the number of taps can increase to give very impractical models. One possibility is to use sparse channel models, in which a large part of the tap coefficients are set to zero. This leads to the situation where the tap delays do not necessarily have to be uniformly distributed. In Sections 4.2.6 and 4.2.7 examples of such models are shown.

4.2.6. GSM model

The multipath behaviour of the mobile radio channel can easily be presented as a tapped delay line model with tap coefficients and delays. ETSI has specified such a model for simple wideband propagation of GSM systems in 1993. The model assumes that the environment is described by highly dispersive multipath caused by large reflectors and/or scatterers along the propagation path. Since the RX is mobile, the angle of arrival is taken into account, since it affects the Doppler shift [ETS93, p.26]. The model is characterised by the number of taps, the time delay relative to the first tap, the average power relative to the strongest tap and Doppler spectrum of each tap. The model consists of two equivalent alternative tap settings, A and B respectively. Three separate tap settings are provided in the model for different environments. The tap setting for rural area is perhaps most relevant to the scope of this thesis, and it is shown in Table 9 [ETS93, p.27]. The tap settings for hilly terrain environment and urban area can be found in Appendix A [ETS93, p.28].

Table 9 Tap setting for rural area.

Tap	Channel A		Channel B		Doppler spectrum
	Relative delay [μs]	Avg. power [dB]	Relative delay [μs]	Avg. power [dB]	
1	0.0	0.0	0.0	0.0	Rice
2	0.1	-4.0	0.2	-2.0	Classical
3	0.2	-8.0	0.4	-10.0	Classical
4	0.3	-12.0	0.6	-20.0	Classical
5	0.4	-16.0	-	-	Classical
6	0.5	-20.0	-	-	Classical

The Classical Doppler spectrum in Table 9 assumes that the arriving signal components are distributed uniformly over all incidence angles, whereas the Rice Doppler spectrum assumes that signal components are Ricean distributed.

4.2.7. UMTS model

The development of UTMS in recent years has created the need for channel models for the 2 GHz frequency band. UTMS operates at a slightly lower centre frequency than WLAN and the modulation bandwidth of UTMS is smaller (5 MHz). Nevertheless, the propagation information of UTMS is also quite appropriate for 2.4 GHz WLAN systems, although the UMTS channel model might not be relevant as such.

ITU has published a recommendation concerning WCDMA channel models. The ITU Recommendation ITU-R M.1225 covers indoor office, outdoor-to-indoor and vehicular environments. The vehicular environment model and its channel impulse response model (based on the tapped delay line model) can be assumed relevant to this thesis. The number of taps, the time delay relative to the first tap, the average power relative to the strongest tap, and the Doppler spectrum of each tap characterize the model. For a majority of time the RMS delay spread is relatively small, but there are occasions with 'worst case' multipath characteristics that lead to a much larger RMS delay spread. These 'worst case' situations occur relatively infrequently, but they can have a major impact on system performance. To model this behavior of the channel, two multipath channels are defined: channel A is the low delay spread case that occurs frequently, channel B is the medium delay spread case that also occurs frequently. Channel A is expected to be encountered 40% of time, while for channel B the value is 55 % of time. Table 10 shows the tapped-delay-line parameters of the vehicular test environment with high antennas [ITU97, p.28].

Table 10 Tapped-delay-line parameters of the vehicular test environment.

Tap	Channel A		Channel B		Doppler spectrum
	Relative delay [ns]	Avg. power [dB]	Relative delay [ns]	Avg. power [dB]	
1	0	0	0	-2.5	Classical
2	310	-1.0	300	-0.0	Classical
3	710	-9.0	8900	-12.8	Classical
4	1090	-10.0	12900	-10.0	Classical
5	1730	-15.0	17100	-25.2	Classical
6	2510	-20.0	20000	-16.0	Classical

4.2.8. Multipath propagation of short-range outdoor radiocommunication (ITU-R P.1411)

Multipath propagation of short-range outdoor radiocommunication is also dealt within ITU-R Recommendation P.1411, which introduces a general model for estimation of delay spread and number of signal components arriving at the receiver.

Estimation of delay spread

The recommendation covers characteristics of multipath delay spread for urban high-rise environment for microcells and picocells (Table 5 and Table 6). The characteristics are based on measurement data at frequencies from 2.5 GHz to 15.75 GHz at distances from 50 to 400 m. The RMS delay spread S at distance d meters follows a normal distribution with the mean value D given by (56) and the standard deviation is given by (57) [ITU03a, p. 14].

$$D = C_a d^{\gamma_a} \ [ns] \tag{56}$$

$$\sigma_S = C_\sigma d^{\gamma_\sigma} \ [ns], \tag{57}$$

where C_a, C_σ, γ_a and γ_σ depend on the antenna height and the propagation environment. Some typical values of coefficients for distances 50 to 400 m are listed in Table 11 [ITU03a, p. 14].

Table 11 Typical coefficients for the distance characteristics of RMS delay spread.

Measurement conditions				D		σ_S	
Area	f (GHz)	h_b(m)	h_m(m)	Ca	γ_a	C_σ	γ_σ
Urban	2.5	6.0	3.0	55	0.27	12	0.32
	3.35-15.75	4.0	2.7	23	0.26	5.5	0.35
			1.6	10	0.51	6.1	0.39
	3.35-8.45		0.5				
Residential	3.35	4.0	2.7	2.1	0.53	0.54	0.77
	3.35-15.75		1.6	5.9	0.32	2.0	0.48

The average shape of the delay profile for 2.5 GHz in dB form can be seen in (58) [ITU03a, p. 14].

$$P(t) = P_0 + 50\left(e^{-\frac{t}{\tau}} - 1\right), \tag{58}$$

where P_0 is the peak power (dB) and t is in ns. τ is the decay factor, which for LOS case can be estimated by (59).

$$\tau = S + 266 \tag{59}$$

Characteristics of multipath delay spread for both LOS and NLOS case in an urban high-rise environment for small macro-cells have been developed based on measured data at 1 920-1 980 MHz and 2 110-2 170 MHz using omni-directional antennas. The medium RMS delay spread S in this environment is given by (60) [ITU03a, p. 15].

$$S_u = e^{(AL+B)} \tag{60}$$

where $A = 0.038$, $B = 2.3$ and L is path loss (dB).

Number of signal components

The number of signal components (i.e. a dominant component plus multipath components) can be identified from the delay profile as the number of peaks whose amplitudes are within A dB of the highest peak and above the noise floor.

Table 12 [ITU03a, p. 17] shows the number of signal components for one scenario (a low BS antenna in a residential area). These figures are based on measurements and published in ITU-R P.1411-2. The temporal resolution in the measurements was 20 ns. Table 13 [ITU03a, p. 17] shows the results of measurements for a high BS antenna in a suburban environment. The temporal resolution in these measurements was 50 ns. These tables list the maximum

number of signal components which have been observed at 80% and 95% of locations in each measurement section.

Table 12 Maximum number of signal components for a low BS antenna in an urban area.

Freq (GHz)	Antenna height (m)		Range (m)	Maximum number of components					
				A = 3 dB		A = 5 dB		A = 10 dB	
	h_b	h_m		80%	95%	80%	95%	80%	95%
3.35	4	2.7	0-480	2	2	2	2	2	3

Table 13 Maximum number of signal components for a high BS antenna in a suburban area.

Freq (GHz)	Antenna height (m)		Range (m)	Maximum number of components					
				A = 3 dB		A = 5 dB		A = 10 dB	
	h_b	h_m		80%	95%	80%	95%	80%	95%
3.67	40	2.7	0-5000	1	2	1	3	3	5

5. Channel modelling methods

The use of more complex communication techniques and smaller cell sizes has generated a need for the detailed understanding of radio propagation in complicated multipath channels. It is important for developers of communication systems to understand the radio wave propagation environment that their systems are facing. Therefore, interest for detailed channel modelling has grown substantially. Even though a lot of research is done in this field, it is still common that some sort of channel modelling is performed in the research and development process. This is due to the fact that the detailed small-scale channel models are accurate in detail only for the specific locations used in modelling, as explained in Chapter 4.

The methods for channel modelling can be divided into two categories: methods based on empirical measurements and computer-aided methods. The traditional way of estimating the channel is naturally various types of measurements but the increased calculation capacity of computers has made significant changes in both types of methods. The methods based on empirical measurements require heavy measurement campaigns and a substantial amount of statistical post-processing of results. These methods usually require expensive equipment and a lot of time, while computer-aided methods focus on simulations of the same channel. Computer-aided methods require heavy calculation capacity, and there still is a need to verify these results with actual measurements [Kal98, p. 21].

5.1. Computer-aided propagation prediction

Computer-aided propagation prediction, or deterministic modelling, intends to reproduce the actual physical wave propagation process for a given environment. Depending on the modelling approach, wideband analyses can be performed including delay, angle of transmission and arrival, as well as polarisation information for each propagation path. In order to obtain deterministic propagation predictions, suitable formulations of the physical propagation phenomena and effects are applied to deterministically described scenarios. The description of the propagation environment can be performed by 3D-vector databases or topographic raster data etc. [COS01, p.132]. Exact modelling of a certain environment produced by deterministic modelling, is perhaps not very useful for more general channel modelling purposes, like in this thesis. Nevertheless, some applications of computer-aided propagation prediction are briefly presented next.

5.1.1. Ray-tracing method

Ray-tracing is a ray-optical based method [COS01, p.143] where the radio wave is assumed to propagate in the same way as a ray of light. The ray-tracing simulation technique incorporates site-specific environment information to predict path loss and delay spread in urban microcells. Using simplified geometric-optics assumptions, rays are traced in three dimensions.

The method determines the path by which direct, specularly reflected, scattered and diffracted rays arrive at a receiver. The rays, which represent local plane waves of the total field radiated by the transmitting antenna, originate from point sources and propagate in three-dimensional space. The received rays are combined noncoherently, as a function of delay, to estimate the channel power-delay profile [Sch94, p.25].

The method is implemented by a simulator that uses pre-determined environment information. Usually several assumptions are made in the propagation calculations. Buildings and ground are assumed to be smooth and perfectly conducting [Bro95, p. 373] and details are simplified to not having many scattering or diffracting items as this significantly decreases the burden of calculations. The increase of calculation capacity has made it possible to use a somewhat more detailed environment for ray-tracing predictions in recent years. An example of such is a new 3-D model in which all buildings and the terrain are formed from triangular planes [Che02, p. 201].

A ray-tracing simulator developed by South-western Bell Technology Resources Inc. and Virginia Polytechnic Institute in 1994 is used as an example in this thesis, to illustrate how such a simulator works. More detailed information of the simulator can be found in [Sch94]. The simulator uses ray-tracing to identify each ray path by which significant levels of energy, radiated from the transmitter, reach the specified receiving point. Initially, the simulator checks for the existence of a line-of-sight path between the RX and the TX. Next, the program generates and traces a ray from the TX in a predetermined direction, and detects if it intersects an object specified in the environment database. If no intersection is found, the process stops, and a new source ray is initiated. If an intersection occurs, the program determines if a scattered ray has an unobstructed path from the intersection point to the RX. The specularly reflected rays are then traced. Each ray is analysed in a similar fashion. This recursive generation and tracing continues until, for each ray, an intersection with the receiver occurs, the maximum number of intersections with objects prior to reaching the RX is exceeded, the ray energy falls below a specified threshold level or no further intersections occur. The scattered rays which do not intersect with the RX are not traced recursively, since the amplitude of these rays

decreases rapidly with distance [Che94, pp. 28-29]. Figure 20 illustrates some typical ray-tracing results.

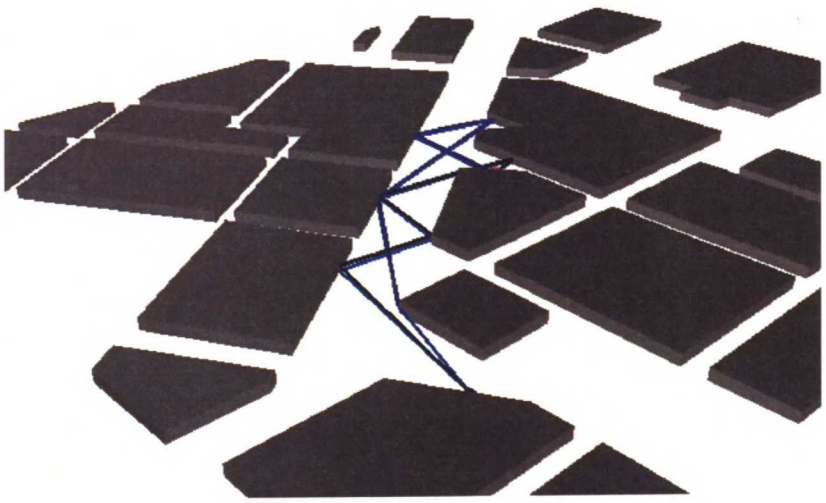

Figure 20 Example of ray-traced 3-D propagation paths between RX and TX using RPS simulation software

Also 2-D ray-tracing can be performed when the antennas are assumed to be below roof-level and no energy is therefore received over the roof-tops. This will reduce the calculation capacity needed but also reduces the accuracy of the results obtained.

Ray-tracing is a suitable computer-aided channel prediction method for urban microcell environments if accurate building and environment data is available. Nevertheless, ray-tracing is not an optimum choice for predicting the channel behaviour in vegetation environment, since the scattering caused by leaves and branches is really hard to model and requires much more calculation capacity compared to urban environment. Also many additional details in reflecting surfaces result in a need for more calculation capacity. In practice these reasons make ray-tracing an impractical propagation method for other than indoor or urban environments.

5.1.2. Methods based on electromagnetic theory

Methods based on electromagnetic theory generate similar results as ray-tracing, while they are based directly on electromagnetism and Maxwell's equations. Finite difference time-domain (FDTD) and Finite-element method (FEM) are well known examples of these methods.

FDTD technique is a powerful numerical method for solving complex electromagnetic problems. It can show the angle of arrival and time delay spread for radio waves propagating in complex environments [Lit96, p.930]. It is

a grid based electromagnetic solver that uses a finite difference scheme to discretise Maxwell's equations in both time and space domains. With FDTD, electromagnetic problems can be simulated at the nodes of the discretised domain. FDTD and its development are presented thoroughly in [Taf95]. For example FDTD is suitable for modelling lift car propagation, which is presented in [Mes99].

FEM is a method that is used for analysing the propagation behaviour of radio waves in special situations and small details like cracks and cavities of the reflecting surfaces [She00]. FEM analysis is also numerical and is based on electromagnetism and Maxwell's equations. The method is presented thoroughly in [Jin93].

5.2. Empirical channel modelling

In contrast to computer-aided propagation prediction methods, which are based on the more or less detailed reproduction of the actual physical wave propagation process, empirical models attempt to reproduce certain characteristics observed from measurements of the radio channel. These characteristics can be derived either directly from the measurement result data or by statistical post-processing of the measurement results, depending on the type of the characteristics. Such characteristics include e.g. average path loss, shadowing loss, delay spread, coherence bandwidth, coherence time, and Doppler-spread as explained in Chapter 4.

This section introduces the measurement process of different kinds of measurements. Even though these methods are applicable to indoors as well, in this thesis, the emphasis is on outdoor environment measurements.

5.2.1. Narrowband measurements

Narrowband measurements are probably the easiest measurements in empirical channel modelling. Distance path loss and shadowing loss models are closely related and are common results of narrowband measurements. These models also represent the easiest way to model a channel empirically.

The measurement process is simple. The equipment needed consists of a transmitter that is located at a fixed point and a receiver that is able to measure the power level (e.g. RSSI) of the received signal. The BS is set to broadcast a cyclic signal using constant transmit power and an omni-directional antenna. In theory the measurements are taken so that the receiver moves along a circle at constant distance away from the transmitter. In practice it is rarely possible to move along a circle due to building location etc. and this need to be taken account in the post-processing of the results. Shadowing is caused by large

obstacles and in addition, the environment may consist of multiple moving and scattering objects that cause time-variant multipath propagation. Therefore the channel is assumed to be nonstatic during the measurements. As a result, multiple measures need to be taken at each point and these results are then averaged to filter away the deep notches and peaks caused by multipath propagation components. The averaging of measurement results is performed by normalising to the local mean. The local mean for every point is obtained by averaging the measurement results symmetrically adjacent to the selected point [Cla68, p. 985]. The local mean follows a certain distribution with some standard deviation. If the assumption that the field is completely scattered is fulfilled, then the expected envelope will follow the Rayleigh distribution with time-varying root-mean square standard deviation $\sigma(t)$. The envelope is now classed as a nonstationary Rayleigh process [Cla68, p. 984].

It is obvious that different locations along the circle have different kinds of propagation environments and produce different losses for shadowing. As a result, shadowing losses are environment specific. Figure 21 illustrates different shadowing environments in locations 1, 2 and 3.

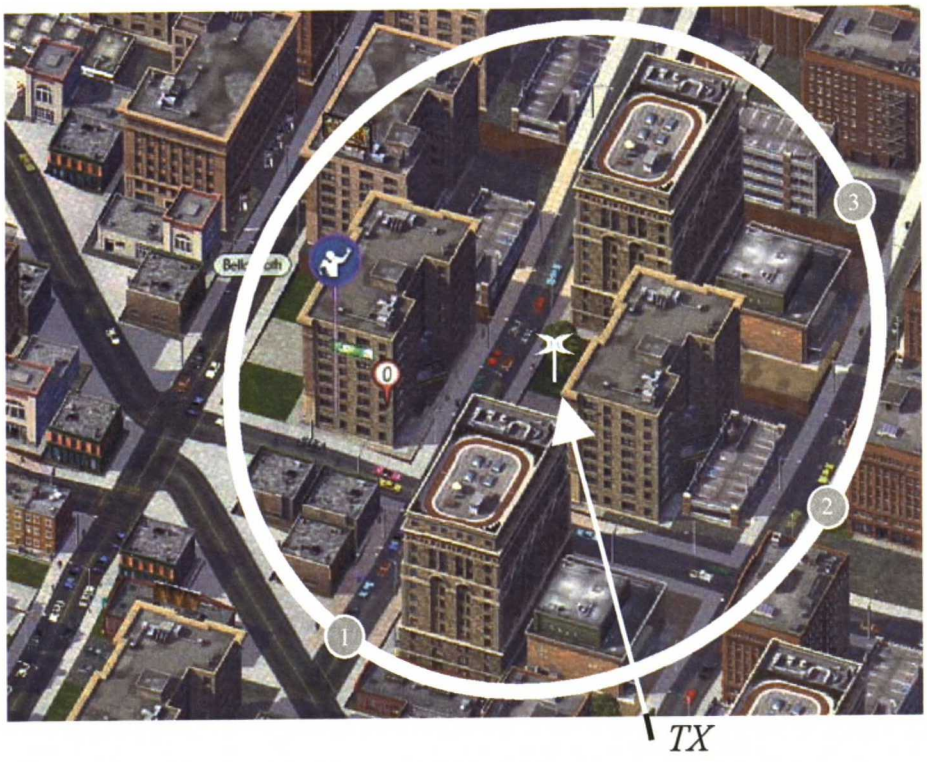

Figure 21 Different shadowing environments in urban environment.

Measurements can then be diversified by taking into consideration a new variable: distance. Additional measurement locations are selected at various distances. Then in addition of averaging results to the local mean, local means

at the same distance are averaged one more time to obtain another local mean, the local mean at a certain distance. Once again the type of environment plays a significant role in the measurements and the accuracy of the measurements decreases when results from different environments are averaged at a certain distance. A certain amount of measurement results is therefore needed.

These measurements are used for obtaining the path loss model of the radio channel as a function of increasing distance between TX and RX or shadowing loss models for different shadowing environments by averaging the results in different ways.

5.2.2. Wideband measurements

A reliable wideband measurement of multipath propagation of a radio channel requires a heavy measurement campaign and highly advanced equipment. Commonly multipath propagation is measured using a specific channel sounder. Sounders are based on separate transmitter and receiver. Basically a short pulse is transmitted by the TX and the received components are observed. The received data needs to be collected using high resolution pulse measuring systems, which increases the required bandwidth. The system makes use of the correlation properties of a pseudorandom shift register sequences to produce low data recording bandwidths for high resolution time-delay measurements. Before transmitting, the signal is convolved with a pseudorandom sequence. The received signal is correlated with the same pseudorandom sequence in a so called sliding correlator. This method was first introduced in 1972 by D.C. Cox [Cox72], who performed multipath propagation measurements at 910 MHz in suburban environment and later in Manhattan, New York. Since then, sounders have been developed and some manufacturers also advertise commercial equipment but this is still not very common, probably due to the high purchasing cost.

Measuring system

Sounder equipment using the same methods as presented by Cox has been developed in Helsinki University of Technology by Radio laboratory and Communications laboratory in the late 1990's. In this thesis this equipment is presented as an example. Even though it was originally designed for 2 GHz, it is quite representative in this field and suitable for the coverage of this thesis. The system is presented in greater detail in [Kiv99].

The measurement system using the direct sequence (DS) method consists of a pseudo-noise (PN) coded transmitter and a correlation detector receiver which is controlled by a PC. Both RX and TX can be used as mobile units because of their moderate size and weight.

In the transmitter the carrier is modulated by the m-sequence generated in the PN generator, which can generate m-sequences of length 31-2047 chips. The chip rates f_{chip} between 2.5 MHz to 60 MHz can be generated by a digital phase locked loop, PLL. Within this parameter range the measured delay (516 ns – 818 µs) and resolution (16.7 ns – 400 ns) can be varied according to the environment. A double-balanced microwave mixer is used as a 2-PSK modulator. Linear output power up to +40 dBm can be transmitted. Figure 22 illustrates the block diagram of the transmitter [Kiv99, p.40].

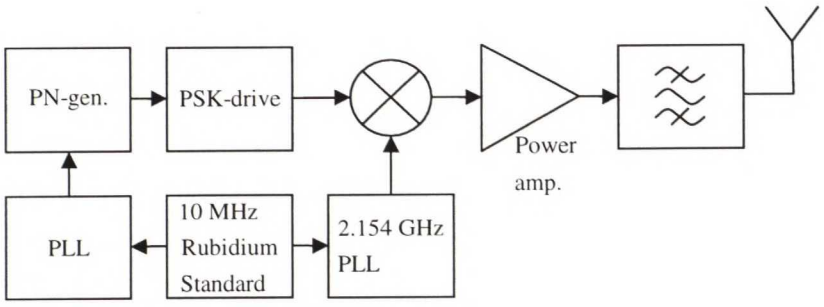

Figure 22 Block diagram of the transmitter.

In the receiver RF front-end, the antenna signal is filtered $(B = 100MHz)$, amplified in a low-noise amplifier and down-converted to intermediate frequency $(IF = 300MHz)$ with a total single-sideband noise figure of 2.5 dB. The IF-stage includes automatic gain control (AGC) with computer-controlled digital step attenuators having a dynamic range of 72 dB, and a major part of the signal amplification. Figure 23 illustrates the block diagram of the receiver [Kiv99, p. 40]. Synchronisation of RX and TX is done using 10 MHz Rubidium standards.

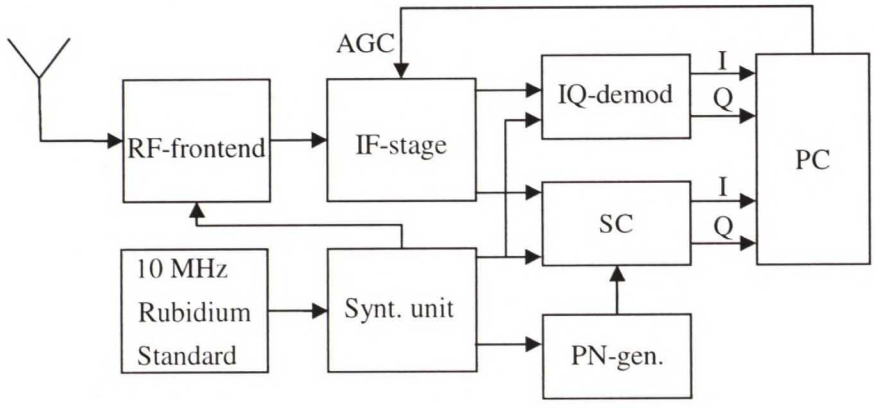

Figure 23 Block diagram of the receiver.

The performance of the DS channel sounder is based on baseband waveform autocorrelation properties. The autocorrelation $R_s(\tau)$ of the periodic signal $s(t)$ with period T_s is defined as shown in (61).

$$R_s(\tau)=\frac{1}{T_s}\int_0^{T_s} s(t)s^*(t-\tau)dt \tag{61}$$

The wideband correlator implementation consists of two alternatives: a sliding correlator (SC) or a matched filter (MF) detector can be used as correlation detector. Using a sliding correlator is the simplest way of implementing such a correlator, since it eliminates the need for rapid sampling and digital processing. Matched filtering is implemented by digital signal processing (DSP) methods. However, in recent years the sliding correlator has been removed from the system and the measurements are based entirely on the DSP configuration.

1) Sliding correlator configuration: In the sliding correlator, a replica of the transmitted m-sequence is generated with a chip rate $f_{chip}^{'}$. The scaling factor K is defined using the difference of the TX and RX chip rates:

$$K=\frac{f_{chip}}{f_{chip}-f_{chip}^{'}} \tag{62}$$

The RX sequence is up-converted to IF and correlated with the received signal. The complex output of the SC, $r^{'}(t)$, is the convolution of the impulse response and cross-correlation of the RX and RX baseband signals, is shown in (63).

$$r^{'}(t)=h(\tau,t)\otimes R_S^{'}(t) \tag{63}$$

Bandwidth compression by the amount of K is achieved at the cost of measurement time. The Maximum measurable Doppler frequency $f_{D,\max}$ is limited to a few tens of Hertz. Thus, the SC has a K-dependent trade-off between $f_{D,\max}$ and the dynamic range of the IR. The measured thermal noise floor is also reduced by K. As an example, if $K=1077$ the IR has a 25 dB dynamic range and the thermal noise floor is at -120 dBm. The in-phase (I) and quadrature (Q) time/bandwidth scaled IR components are A/D converted to 12 bit with maximum 2 x 500 kHz sampling rate. The data is stored to a mass memory of the PC and therefore the length of the measurement is limited to the size of the mass memory.

2) DSP configuration: In the DSP configuration, the IF signal is converted to the baseband in the IQ-demodulator, and the baseband signal is sampled with 2 x 125Ms/s maximum sampling rate on an 8-bit dual-channel sampling board. The information is buffered to a buffer memory and finally transferred to a PC. Typically data for a few IR's is sampled at a time and the signal-to-noise ratio is improved by averaging. The complex IR is then obtained from the raw data by

off-line processing. The received complex baseband signal $r(t)$ is convolved with $m_s(t)$, which is the impulse response matched to the used m-sequence, as shown in (64).

$$h(\tau,t) = m_s(t) \otimes r(t) \tag{64}$$

In Figure 24 the receiver of the measurement equipment is on a movable trolley equipped with spherical antenna and ready for measurements.

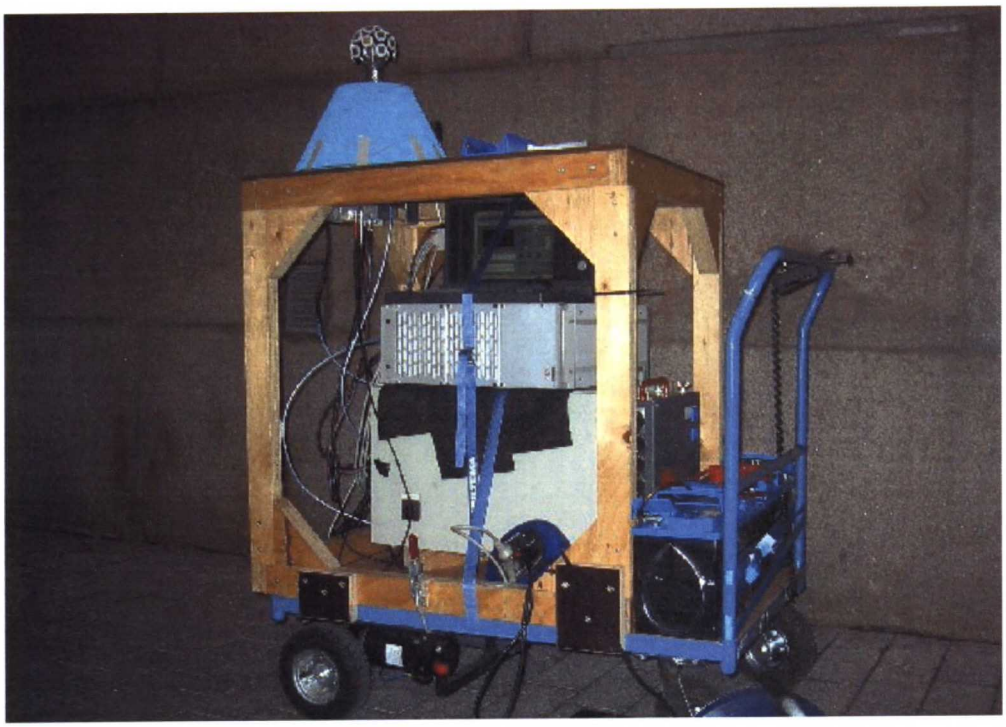

Figure 24 Receiver of the HUT sounder on a trolley and ready for measurements.

Measurement process requirements

As an example of a successful measurement process, measurements conducted by the Radio laboratory of Helsinki University of Technology in the centre of Helsinki at 2 GHz in 2000 are presented. The process in greater detail can be found in [Vuo01]. The measurements were conducted in five environments, all located in the centre of Helsinki. The sounder receiver was moved slowly on a small trolley in the streets of Helsinki. Night time was chosen to decrease the amount of traffic and movement in the streets to be able to conduct the measurements in as static a channel as possible. The routes had different lengths varying from 115 to 400 metres and distances between RX and TX varying between 100 to 630 metres.

A 32-dual polarisation element antenna shaped as a sphere was used in the measurements. The same shape is used in footballs. The 6 dB beam width of

each antenna element is 90° (vertical) and 100° (horizontal) and the antenna gain is 7.8 dB. With this antenna also the polarisation and the direction of incidence of the received signal can be specified. When using such an antenna array, each element is measured separately by switching the elements in turn using a fast RF-switch. In addition the phase, delay and amplitude of each propagation path is detected.

The real-time data storing makes it possible to measure samples of the channel with very small intervals. Therefore, the RX can be moved during the measurement and the channel along even long measurement paths can be measured relatively quickly. Condition to mobility and certainty of the measurement results is that the channel can be considered static over the time of the measurement. The channel is assumed static if the receiver moves only an insignificant amount of wavelengths during one measurement period. Also following from the Nyquist criterion, more than two measurement samples must be obtained over a wavelength. For example the acquisition time of two consecutive impulse responses (two samples are needed for averaging reasons) takes 0.54 ms using 32-element antenna, 127 bit PN-code and two polarisations with this equipment [Vuo01, p.39]. For example if the receiver moves at a velocity of 1.0 m/s, it moves 0.54 mm over one measurement period. The movement of the receiver corresponds to about 1/4000 of the wavelength at 2 GHz.

The actual measurement process is conducted within these requirements by moving the receiver at a constant speed along the intended route. The transmitter is located at a fixed position with constant transmit power. The sounder gathers a substantial amount of impulse responses in the form of raw data in the PC. This data can be imported e.g. to Matlab for post-processing and analysing. The system functions and characteristics of the radio channel can be obtained by using the methods described in Section 4.2.2. Figure 25 and Figure 26 show some examples of results of a multipath propagation measurement campaign as described above.

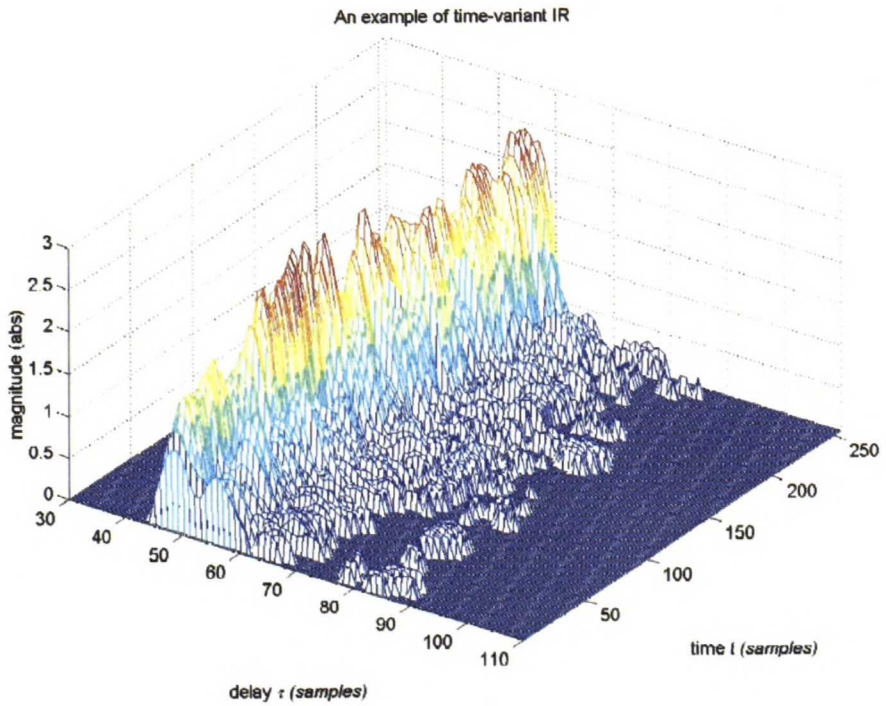

Figure 25 Example of time-variant impulse response measured in Tapiola, Espoo at 2 GHz.

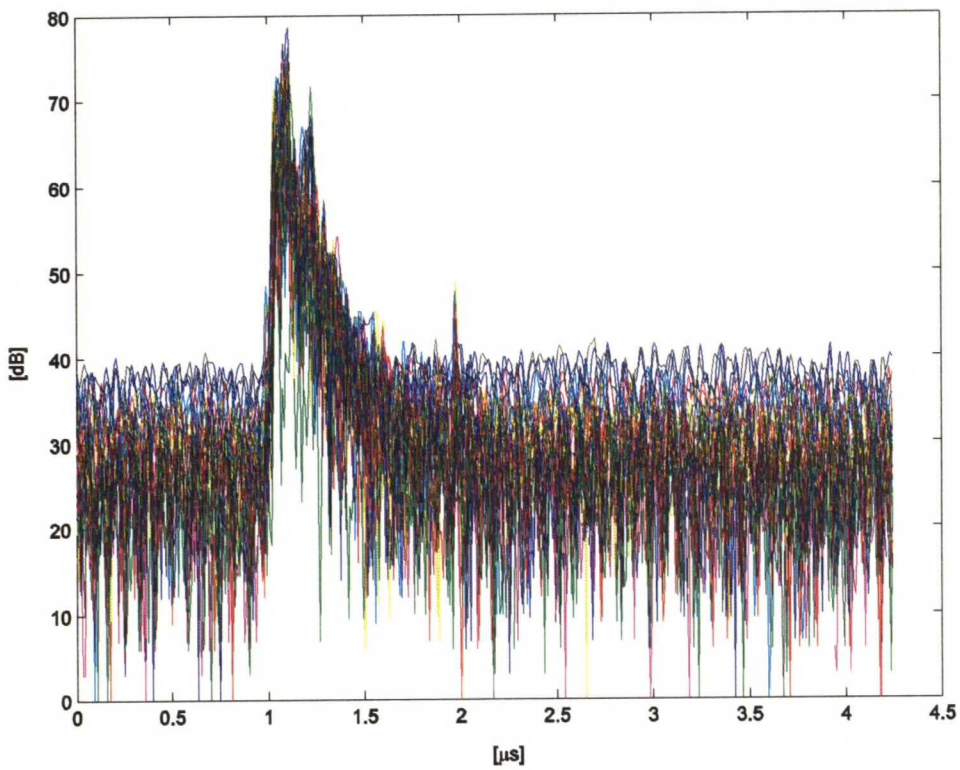

Figure 26 Impulse response measured in Fabianinkatu, Helsinki at 5 GHz. IRs from all RX antenna elements are plotted on top of each other. TX was located on the roof of a building 30 m directly above the RX.

6. Channel modelling of WLAN systems

There are multiple choices how the actual channel modelling is performed. In this chapter the methods presented above are applied to WLAN systems. The methods vary from theoretical models to simulation and heavy measurements depending on the accuracy of the results needed and the resources available.

Whereas the existing channel models provide an easy approach to the task, they merely consist of large-scale models. The lack of small-scale propagation prediction results in inaccurateness of the achievable results. Even yet, the large-scale models do not cover precise WLAN frequencies at 2.4 GHz and only the Hata model covers environments other than urban. Neither do these large-scale models take into account the effect of vegetation; one needs to consider these using an additional vegetation model.

Small-scale propagation models also lack a proper model for WLAN operating at 2.4 GHz, even though a lot of measurements have been conducted at 2 GHz for the development of UMTS. There are many results of sounder measurement campaigns available in the books and scientific journals also at 2.4 GHz, but they are mainly in urban environment or indoors. As a result, when an accurate multipath propagation channel model for WLAN systems operating in different types of outdoor environments (e.g. suburban, rural etc.) containing also vegetation is needed, the only possibility available at the time of writing this thesis is to conduct the channel modelling.

Even though computer-aided propagation prediction methods can be useful in many situations, they prove to be infeasible for environments containing vegetation, due to the difficulties of modelling the scattering caused by leaves and branches. Also to be able to get accurate results with e.g. the ray-tracing method, a huge calculation capacity is needed. The amount of details in surrounding surfaces increases the needed calculation capacity even further. In practice, any other than solid box-shaped buildings increases the needed capacity and calculation time too much. If these methods are still applied, the results need to be verified by conducting some actual empirical measurements. As a result, computer-aided propagation prediction proves to be infeasible.

As a conclusion, it seems that a heavy measurement campaign is inevitable. Nevertheless, WLAN system characteristics and impact of different outdoor environments have great influence on the channel measurement process and equipment requirements. These influencing aspects are presented next, and as a conclusion the reader is able to comprehend different aspects of a feasible measurement campaign.

6.1. Impact of different outdoor environments

The characteristics of the environment in hand have a major impact on the measurement process and the measuring equipment. Consider the difference between office-type indoor environment and a big open rural area with only few buildings.

In an office-type indoor environment, there are typically a lot of small rooms with a lot of reflecting surfaces or moving scatterers in the sense of radio wave propagation. The impact of these characteristics results in lots of multipath propagation components with small delay spread (few hundreds nanoseconds). Traditionally, this type of propagating channel is the main application environment for WLAN systems.

On the other hand, a big open rural area with only a few buildings typically results in a dominating line-of-sight component and a few multipath components with large excess delay. In case of shadowing, there is no line-of-sight, but only a few multipath components with large delay spread. As an example, there can be a reflecting surface (e.g. a house) about a kilometre away, so that the reflected component propagates along a path of a length of additional 2000m compared to the LOS component. The reflecting component is delayed by the amount of τ compared to the LOS component.

$$\tau = \frac{2000m}{3.0 \cdot 10^8 m/s} = 3.33\mu s \tag{65}$$

According to free space loss theory, this delayed component is attenuated by the amount shown in (66).

$$L_0 = 32.45 + 20\log(2400MHz) + 20\log(2km) = 106dB \tag{66}$$

Then, the received power level is close to $-80dBm$ if the TX power is the allowed $+20dBm$ (including the gain of receiving antenna). A multipath component with such received power level is well within the WLAN RX dynamic range and above the noise floor $(\approx -90dBm)$, and therefore should be taken into account in the channel modelling process. Because of this feature, the measuring equipment must be able to measure large enough excess delay.

Such differences in the measured environments need to be considered when planning a measurement campaign and setting up measurement equipment requirements. Also the disposition of buildings and other reflecting surfaces, possible moving objects like cars and the type and placement of vegetation need to be considered in the planning phase. An aerial view of the environment

is also a useful tool in planning. Above all, the most important aspect is still the knowledge of the purpose of the measurements and the expectation of the results.

6.2. WLAN signal restrictions and system behaviour

According to the IEEE 802.11 WLAN standard the WLAN signal has bit rates of 1 Mbit/s and 2 Mbit/s using DBPSK and DQPSK modulation, respectively, as mentioned in Chapter 2. Both of these bit rates use a symbol rate of 1 Ms/s, and symbols contain one and two bits in DBPSK and DQPSK, respectively. In IEEE 802.11b additional bit rates of 5.5 Mbit/s and 11 Mbit/s using CCK-modulation are introduced. These modes are using a symbol rate of 1.375 Ms/s [OHa99, p. 154]. This means that the duration of a symbol T_S (or bit in DBPSK case) is:

$$T_S = \frac{1}{R_S} = 1\mu s\,, \tag{67}$$

for DBPSK and DQPSK, and

$$T_S = \frac{1}{1.375 Ms/s} = 727 ns\,, \tag{68}$$

for CCK signals.

As a consequence, the theoretical maximum excess delay that a WLAN receiver is able to comprehend is the duration of a symbol, i.e. 1 µs or 727 ns, regardless of the receiver implementation. If a WLAN signal is used for radio channel modelling measurements, these characteristics result in a major restriction for channel modelling. This is due to the fact that the next symbol will arrive after this period and the receiver is locked to it. Also during the symbol duration there are signal components from the previous symbol causing interference. It is still worth pointing out that the duration of a symbol is theoretical maximum and it is hard to achieve due to the additional processing needed after symbol reception. Also, the receiver implementation may utilise additional delays. Since the receiver implementation is left open in the standard it may vary a lot between manufacturers. As an example, the actual delay spread tolerance achieved by Orinoco in their WLAN PC card can be seen in Table 14 based on [Luc00, p. A-6]. It seems that even at a bit rate of 1 Mbit/s components with only half of the theoretical maximum excess delay are actually taken into account and this amount decreases as the bit rate increases. A delay spread of 500 ns stands for an additional propagation path length of 150 metres, which means e.g. a reflection from the surface 75 meters away. At the 11 Mbit/s bit rate the corresponding lengths are 19.5 meters and 9.75 meters,

respectively. These delay spreads correspond to indoor environment but they are indefinitely too small for outdoor use of the system.

Table 14 Delay spread tolerance of Orinoco WLAN PC Card.

Bit Rate (Modulation)	11 Mbit/s (CCK)	5.5 Mbit/s (CCK)	2 Mbit/s (DQPSK)	1 Mbit/s (DBPSK)
Delay Spread (at FER of < 1%)	65 ns	225 ns	400 ns	500 ns

As a conclusion it is obvious that a WLAN signal is suitable for WLAN channel modelling in indoor environments but for outdoor environments another signal must be selected. As a comparison, in the GSM tapped delay line model for hilly environment, the last tap is delayed by 20 μs as can be seen in Appendix A.

A more significant conclusion is that IEEE 802.11 and IEEE 802.11b WLAN systems will have trouble comprehending signal components arriving with delays more than 1 μs or 727 ns, respectively, without advanced countermeasures since the receiver is busy with the next symbol. Also during this time there arrive signal components from the previous symbol. All the energy received after the delay mentioned, will increase intersymbolic interference (ISI) and noise. This can be a major set-back to WLAN system behaviour if it is used in outdoor environments. It also presents an interesting research subject to measure the amount of energy received after the delay in percentages and its impact on some quality parameter (FER, throughput etc.) on WLAN systems in various environments.

Even though the WLAN signal is not optimal for channel measurements, there are measuring equipments available in the market that exploits it. As an example of such, is the Berkeleys Varitronics Systems Inc.'s Yellowjacket. This measurement tool and its behaviour are presented next as a case study.

6.2.1. Case: Berkeley Varitronics Systems Inc.'s Yellowjacket

Berkeley Varitronics Systems Inc.'s Yellowjacket is a small and handy device, which is built on Compaq IPAQ PocketPC. It's a hand-size mobile measurement tool, which is intended in particular for sweeping, analysing and optimising 2.4 GHz WLAN networks. According to the device's user manual, it is capable of measuring all 14 DSSS network channels, RSSI in dBm for each transmitter, packet error rate (PER), MAC addresses, service set identifier

(SSID) and received multipath components correlated power measurements. The device also includes a spectrum analyser mode. The basic features of the device and general specifications of the receiver are listed in Table 15 [BVS, Appendix].

Table 15 Basic features of Yellowjacket.

Bands supported	ISM: 2.400 – 2.495 GHz
RF dynamic range (wideband)	-20 to -90 dBm
RSSI measurement dynamic range (narrowband)	-30 to -90 dBm @ 343.75 kHz resolution bandwidth
Tuning increments	Tunes to all 14 international channels
Receiver IF sensitivity	-30 to -100 dBm
Stability	± 2.5 PPM Temp range -1°C to 49°C

At first, the system seems very promising. Its features cover multipath analysis, which is based on a correlation receiver. The receiver correlates the received signal with an 11 bit Barker code that is also used in transmission. The investment cost of this device is less than 1 % of the cost of a proper channel sounder, which makes it an attractive device. The multipath analysis is based on a WLAN signal, which restricts the analysis as pointed out in Section 6.2. Nevertheless, the system consists of a WLAN receiver and it should be able to measure WLAN system quality parameters at the same time when analysing the channel. If it could be assumed that the system represents a typical WLAN receiver, WLAN system behaviour in different environments could be easily analysed, even though the channel model would lack information of delay spreads larger than 1 μs. The device is able to save all the measured information in a log file, which makes post-processing possible e.g. by using Matlab.

Test measurements with Yellowjacket

Yellowjacket has been used in outdoor environments for some test measurements before starting a multipath propagation measurement campaign in a larger scope. The test measurements were taken just outside the Department of Electrical and Telecommunication Engineering building, inside the campus area of Helsinki University of Technology, in Espoo. Three simple but different measuring environments were selected to test the properties of the Yellowjacket. The sites were all located outside, consisting of one line-of-sight environment and two non-line-of-sight environments. The NLOS cases were selected so that one had a worse multipath channel and the other was between LOS and the worst NLOS case. Figure 27 illustrates the situation.

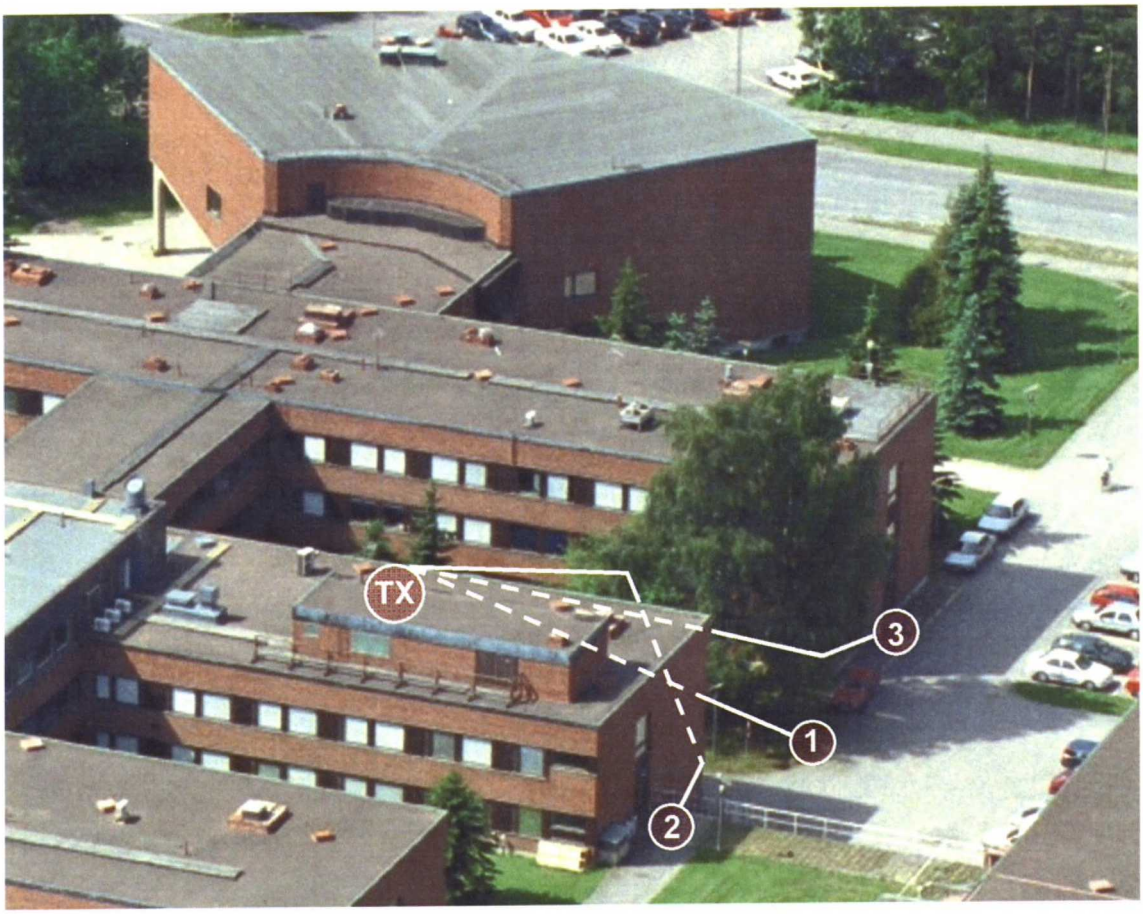

Figure 27 Measurement environment of three test measurement cases.

In Figure 27 the transmitter (i.e. WLAN BS) is located inside on the 3rd floor just inside the window facing the alley in the middle of the figure. Measurement point no. 1 is located in the middle of the alley with direct LOS to the BS. Point no. 2 resembles the worst NLOS case; the measurement point is located under a concrete stairway. Point no. 3 is the less severe NLOS case where the RX is around a corner as seen in the figure. White lines illustrate one possible propagation path to each measurement point.

It is worth pointing out that these test measurements were done to test the functionality of the Yellowjacket device, not to produce actual channel models. Therefore, only one sample of each case was enough to see the effect on the Yellowjacket of different propagation environments. Before even starting to analyse the measurement results, the first major set-back in the functionality of the measurement device was identified. In Table 16 a sample of the Yellowjacket log-file can be seen. The log-file is generated in such a way that a row is saved for each packet received. In the log-file, take notice that in the column "good/bad" packet all samples have the value "1". This means that all the packets in the log-file are "good" packets and there is no information available on the "bad" packets. According to the manufacturer, the "bad" packet

information will be included in the software in the future. The conclusion is that Yellowjacket with the software version available at the time of writing is actually incapable of measuring the packet error ratio, or any other quality parameter of the WLAN system.

Table 16 Sample of Yellowjacket log-file.

Ch	RSSI	Multipath data (22 samples)																						Data Rate	Good / Bad
4	-63	4,8	3,8	2,6	1,1	0,3	6,2	27,5	53	61,2	44,5	18,7	4,4	0,4	0,2	0,9	1,7	2,2	1,2	0,2	0,2	0,4	0,3	2 Mb	1
4	-63	4,1	3,4	1,9	1,2	0,7	0,5	9,2	37,9	66,7	62,6	31,8	7,9	1,5	0,7	0	1,4	3,9	3,9	1,9	0,4	0,9	0,9	2 Mb	1
4	-73	7,9	3,8	2,1	1,6	1,5	0,8	6,5	38,5	70,6	49,2	12	9,6	9,7	5,3	0,7	3,2	5,3	3,5	0,5	3,7	6,7	3,1	2 Mb	1
4	-60	6,2	5,2	2,9	1,9	1,7	0,1	5,8	35,4	69,2	64,8	31,3	6,5	0,6	0,3	0,5	1,7	3,6	3,3	0,9	0,1	0,8	0,8	2 Mb	1
4	-62	4,8	2,9	1,7	1,2	0,4	1,9	20,9	57,2	73,4	54	21	5,1	0,9	0,4	0,6	1,8	2,4	2,8	0,3	0,3	0,9	0,5	2 Mb	1
4	-74	3,9	2,9	2,1	1,7	4,1	14,9	28,9	45,8	52,4	38,4	13,7	4	1,5	1,4	1,3	1,4	3,6	3,2	1,1	0,7	0,4	0,3	2 Mb	1
4	-64	6,2	4,2	2,5	2,1	1,3	0,3	11	38,9	62	50	22,9	6	1	0	0,3	2,2	3,4	2,5	0,8	0	0,4	0,3	2 Mb	1
4	-71	3,1	2,7	1,8	1	0	4,8	28,4	58,2	59	29,9	12,3	5,6	2,2	0,4	1,1	3,1	3,9	2,5	0,4	1,7	0,9	0,2	2 Mb	1
4	-65	5,2	3	2,2	1,8	0,3	4,5	28,9	57,9	58,9	31	8,1	1,1	0,1	0,5	1,5	2,9	2,8	1,2	0,2	0,5	0,4	0	2 Mb	1
4	-67	4,4	3,8	2,7	1,9	0,9	0,2	8,9	37,3	58,8	48,6	19,2	3,2	0,3	0,1	0,5	1,8	2,5	1,5	0,2	0,5	1	0,5	2 Mb	1
4	-81	1,2	1,2	1,7	12,7	35,3	33,1	14,1	25,5	40	26,6	8,2	2,9	1,9	2,2	1,3	2,8	7,9	5,7	0,6	1,4	2,3	1,5	2 Mb	1
4	-74	7,8	6,7	2,9	1,5	1,5	0,2	6	37,2	73,1	71,7	37,4	10,5	2,1	0,6	0,6	0,8	2,8	3,4	1,7	0,2	0,7	0,9	2 Mb	1
4	-70	4,3	2,9	1,7	0,9	0,5	0,2	10,8	45,6	72,3	55,7	20,8	3,9	1	0,8	0,3	0,9	1,7	1,5	0,6	0,3	0,7	0,7	2 Mb	1
4	-69	5,2	4,2	2,5	1,7	1	0,1	9,6	44,2	71	57,3	23,7	4,2	0	0	0,8	1,6	2,2	1,8	0,7	0,3	1,1	1,1	2 Mb	1
4	-71	5,3	3,2	2,2	2,1	1	1,7	23,8	61,7	68,6	35,6	8,5	1,1	0,1	0,5	1,6	3,1	4,3	1,8	0,2	1	1,1	0,2	2 Mb	1
4	-70	6,5	5	2,8	2	2,2	0,1	6	37,1	67,9	57,7	26,9	5,9	0,4	0	0,3	1,2	2,8	2,7	0,8	0,3	0,7	0,9	2 Mb	1
4	-67	4,8	3,6	2,5	2,3	1,1	0,4	12,4	44	68,3	57,6	27,3	5,4	1	0,4	0,2	1,2	3,1	3,4	0,8	0,4	0,8	0,3	2 Mb	1
4	-67	5,2	3,5	2,1	1,9	1	1,1	14,1	43,5	59,7	45,2	18,5	4	1	0,5	0,9	2,1	2,7	2,1	0,8	0,1	0,1	0	2 Mb	1
4	-67	4,6	3,2	2,2	2,4	1,7	1,4	17,1	49,2	64,3	45,7	19,6	5	1,3	0,3	0,2	1,9	2,7	3,1	0,9	0	0,2	0,1	2 Mb	1
4	-67	4,5	2,9	2,1	2	0,9	3,2	19,6	47,9	61,2	45,7	20,6	5,5	0,9	0,4	1,3	1,4	2,1	1,7	0,7	0,3	0,7	0,1	2 Mb	1
4	-68	5	3,6	2,4	2,7	1,8	2,4	17,3	47,2	70,2	63,2	31,2	9,3	1,6	0,5	0,7	2,4	3,7	2,3	0,5	0,3	0,6	0,3	2 Mb	1

The multipath data in the log-file consists of 22 samples, which are, according to the manufacturer, samples in ½ chip intervals. It seems that, for each packet, multipath information over a time period of 11 chips is saved to the log-file. A time period of 11 chips corresponds to a symbol length T_S. Even though each packet consists of multiple symbols, multipath information is stored only for one symbol of the packet. It still remains unclear which symbol of the packet this is. For 1 Mbit/s and 2 Mbit/s the ½ chip interval corresponds to a time period of 45 ns and the value is 33 ns for higher bit rates.

Test measurement results and analysis

The multipath data values present correlation values and are not directly comparable. This is due to the fact that the device has automatic gain control (AGC), which tunes the power level of the received symbol to a suitable level

before correlation. According to the manufacturer, the absolute power in each time of arrival window could be calculated using (69).

$$P_i = 10\log\left(\frac{C_i}{C_{\max}}\right) + P_{Ch}, \tag{69}$$

where P_{Ch} is the total channel power (RSSI), C_i is the multipath data correlation value and $C_{\max}$ is the perfect quality total multipath number. The value of $C_{\max}$ was determined by measurements to be $C_{\max} = 2709.6$. This measurement was performed by connecting an access point to Yellowjacket by cable.

The impulse response of the three different multipath propagation cases produced from the multipath data with corrected absolute power levels of these 22 samples in the delay domain (corresponds to $T_s = 1\mu s$ since a 2 Mbit/s bit rate was used) and various amount of samples in the time domain can be seen in Figure 28, Figure 29 and Figure 30.

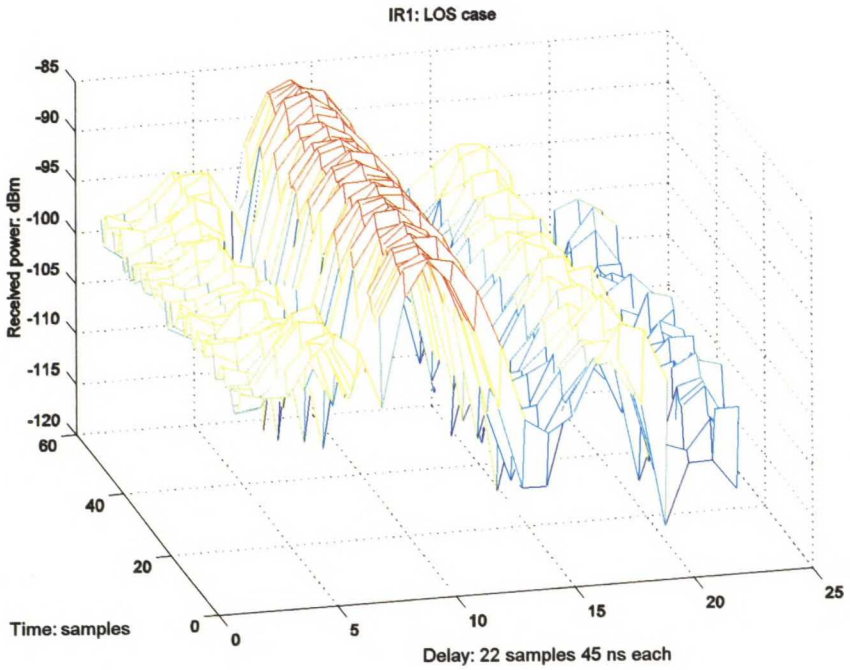

Figure 28 Impulse response of LOS case.

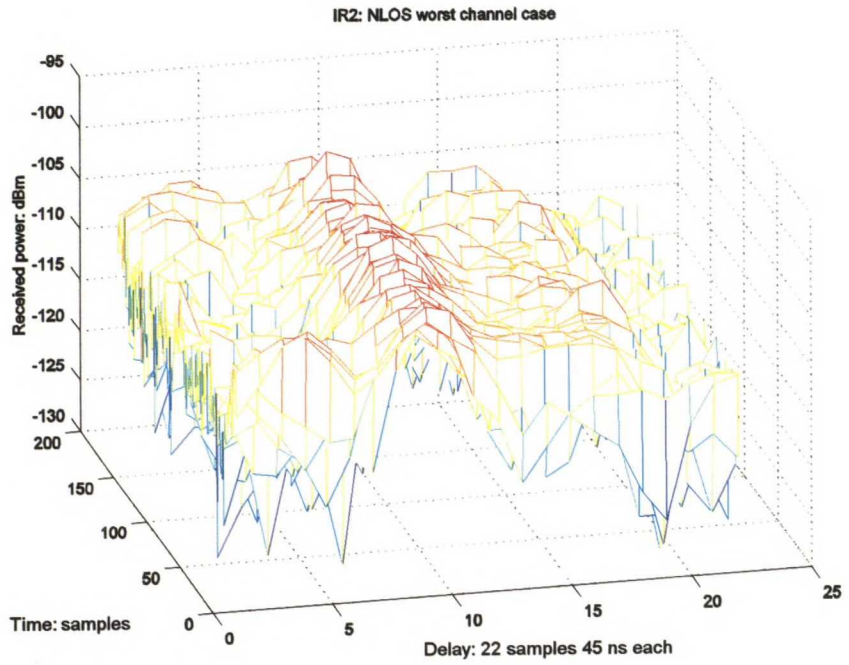

Figure 29 Impulse response of the worst NLOS case.

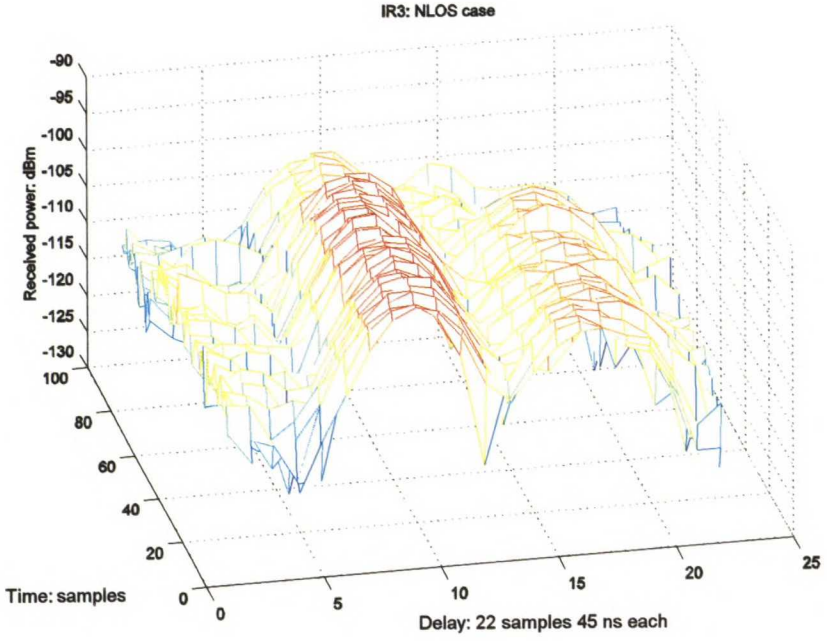

Figure 30 Impulse response of the other NLOS case.

From the figures it can be seen that the test measurements differentiate in the way they should: in Figure 28 the LOS component in clearly visible, in Figure 29 the received power is distributed over the entire delay spread area available, and the impulse response in Figure 30 seems to be in-between the ones seen in the previous figures, as expected. Still there is something suspiciously similar in these impulse responses. For further analysis the results are averaged over

the time domain, and these averaged impulse responses with absolute received power levels can be seen in Figure 31, Figure 32 and Figure 33.

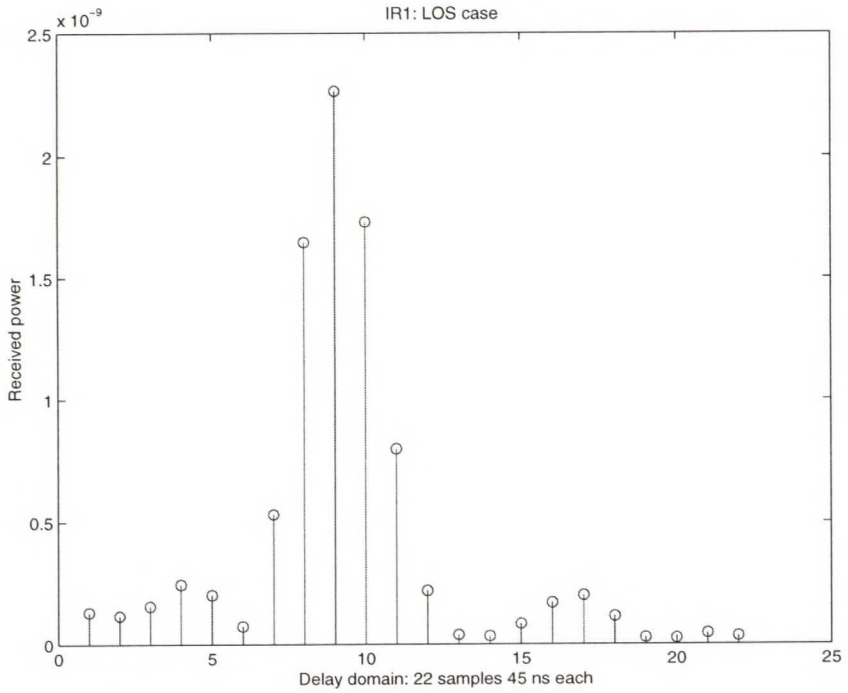

Figure 31 Impulse response of the LOS case averaged over the time domain.

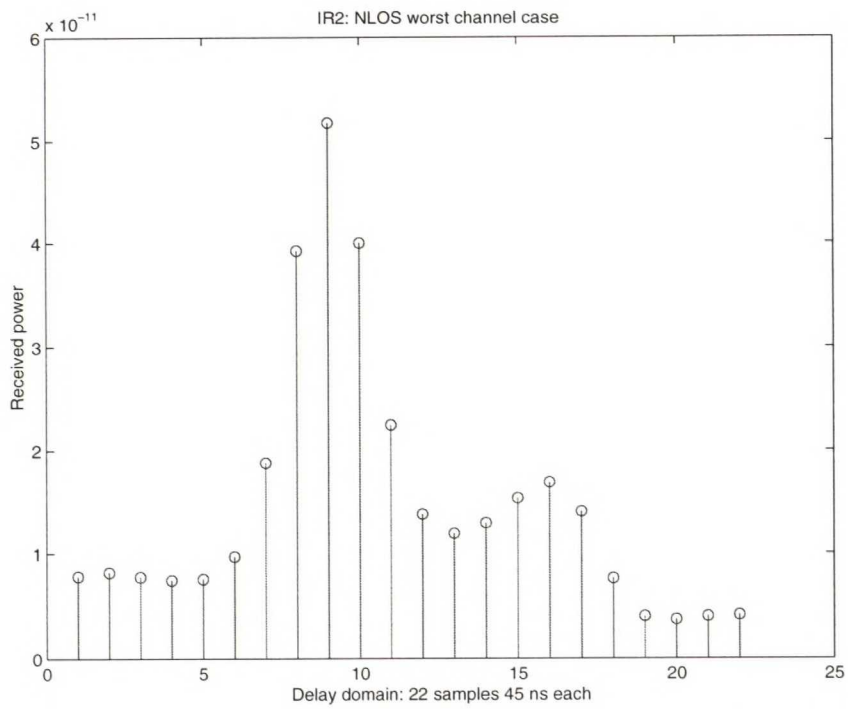

Figure 32 Impulse response of the worst NLOS case averaged over the time domain.

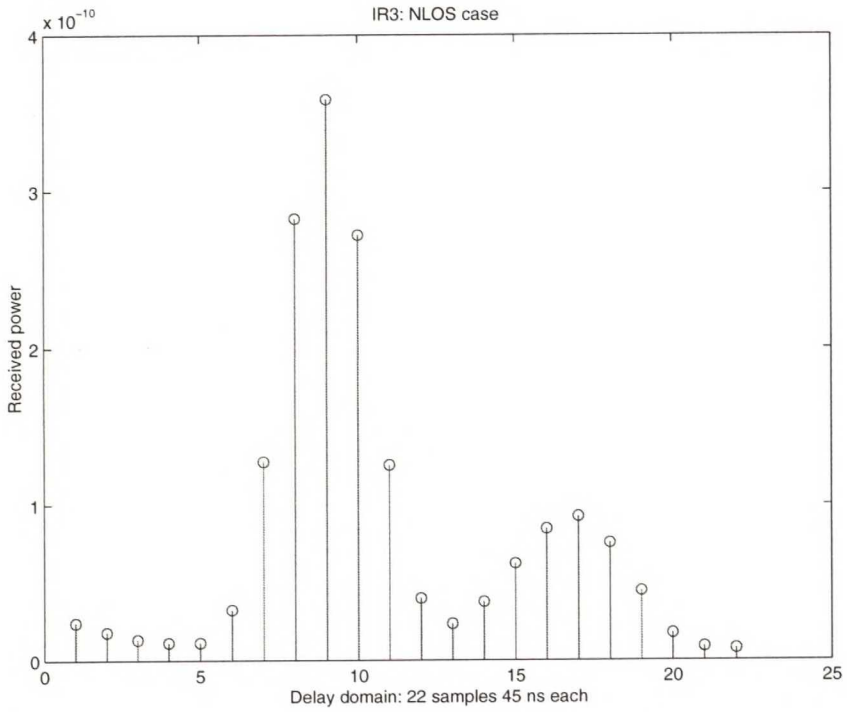

Figure 33 Impulse response of the other NLOS case averaged over the time domain.

Three important observations can be made from these figures. First, the strongest component seems to be located on the 9th sample. This is interesting, considering that there ought to be different propagation delays between LOS case and NLOS cases. It seems that the receiver always locks to the strongest component and its peak value is located in the 9th sample. This characteristic makes this device inapplicable to channel measurements requiring absolute delays of the components. With this device there is absolutely no information available of the propagation delay before the strongest component. Nevertheless, the receiver is not synchronised to the transmitter in any way, so it is not a big surprise that the information mentioned is missing.

Secondly, because the peak value is found at the 9th sample it is obvious that the first eight samples contain very little information and they can be filtered away. This results in an even further degradation of the delay spread window; from 1 μs to 640 ns.

The third and most inconvenient observation focuses on the shape of the impulse responses. All IRs consist of two "hills", even though uncorrelated taps are expected. This indicates heavy filtering with a too narrow band-pass filter. This result in correlation between measured samples and samples cannot be assumed independent. Yet still, these hills seem to be located approximately same distance apart (8 samples, i.e. 360 ns) in each impulse response. It actually seems that the measurement results are in fact two consecutive impulse responses of the band-pass filter that gathers all the energy within the

bandwidth of the filter. The bandwidth of the filter is concluded to be about $11Mchip/s/4chip = 2.75MHz$, while the baseband bandwidth of the signal is $11Mchip/s$. The bandwidth of the RF-signal is 22 MHz, due to the modulation spread.

It is obvious that the delay between the hills is unreliable. As a result Yellowjacket is only capable of producing measurement results for a tapped delay line channel model consisting of two independent taps, with unreliable fixed delay between them. After the test measurements there was no reason to pursue measurements any further with this measurement device. On the other hand, Yellowjacket later proved to be a nifty little gadget in finding network failures and interference sources, but it cannot be used as a substitute to a channel sounder system.

6.3. Summary of channel modelling of WLAN systems

Even though there are many alternatives of performing channel modelling in general, in this case wideband measurements seem inevitable, since existing channel models and computer-aided methods do not provide any help for WLAN channel modelling in outdoor environments outside urban city. The environment and its characteristics play a significant role in measurement planning as it can have a major impact on the excess delays and multipath propagation. It is obvious that IEEE 802.11 or IEEE 802.11b WLAN signals are unsuitable for such measurements because excess delays larger than 1 μs or 727 ns cannot be measured. This characteristic is also a major restriction to WLAN usage in general. The measurements should be conducted with proper sounder equipment, even though the investment costs of such equipment are substantial. An example of suitable commercial equipment is PROPSound by the Elektrobit Group. At the time of writing this thesis there is no substitutive commercial equipment available on the market as the most promising measurement tool, BVS's Yellowjacket, proved to be unusable.

7. Conclusions

The purpose of this thesis was to study the process of determining wideband radio channel models for WLAN systems in different outdoor environments. Different outdoor environments are outside the scope of the traditional operating conditions of WLAN systems. From a radio wave propagation point of view such environments exhibit very different propagation conditions due to for example vegetation, large delay spreads and perhaps fewer multipath components. The main focus was on the IEEE 802.11b WLAN system. The study was conducted as a review of WLAN techniques and their characteristics, theoretical investigations of the radio wave propagation phenomena, a literature research on existing channel models and an investigation and review of different general channel modelling methods. The results from this theoretical part were then applied to WLAN system channel modelling by inspecting the impact of different environments, WLAN signal characteristics and empirical measurements with one possible measurement tool: BVS's Yellowjacket.

There are multiple choices on how the actual channel modelling is performed. The basic radio wave propagation mechanisms form the basis of all propagation modelling. Whereas the existing channel models provide an easy approach to the task, the only directly applicable models found were merely large-scale models. Even yet, the large-scale models do not cover precise WLAN frequencies and only the Hata model covers environments outside the urban city. Neither do these large-scale models take into account the effects of vegetation; one needs to consider these using an additional vegetation model.

Small-scale propagation models also lack a proper model for WLAN operating at 2.4 GHz, even though a lot of measurements are conducted at 2 GHz for the development of UMTS. There are many results of sounder measurement campaigns available in books and journal articles also at 2.4 GHz, but they are mainly performed in an urban environment or indoors. The lack of suitable small-scale propagation prediction models leads to the need of conducting channel modelling, especially when an accurate multipath propagation channel model for WLAN systems containing the effects of different types of outdoor environments (e.g. suburban, rural etc.) and vegetation is needed.

Even though computer-aided propagation prediction methods can be useful in many situations, they prove to be infeasible for environments containing vegetation due to the difficulties of modelling the scattering caused by leaves and branches. Also to be able to get accurate results with, e.g. the ray-tracing method, a huge calculation capacity is needed. The amount of details in surrounding surfaces increases the needed calculation capacity even further. In

practice, any other than solid box-shaped buildings increases the needed capacity and calculation time excessively. If these methods are still applied, the results need to be verified by some actual empirical measurements. As a result, also computer-aided propagation prediction proves to be infeasible, also.

In conclusion, it seems that a heavy measurement campaign is inevitable. Nevertheless, WLAN system characteristics and the impact of different outdoor environments have a great influence on the channel measurement process and equipment requirements. WLAN signals proved to be unsuitable for radio channel sounding purposes if longer delay spreads than 1 μs (IEEE 802.11, 727 ns for IEEE 802.11b) are needed, as is almost always the case with target outdoor channels. The measurement system should be wideband enough not to filter the signal used in the sounding process. Also, fast data acquisition is needed if a mobile channel is to be modelled. Only then is it possible to move the receiver without decreasing the accuracy of the results.

7.1. Future work

After this thesis it is clear that a wideband radio channel sounding measurement campaign must be done in order to be able to produce the actual channel model. The channel measurements should be conducted in all interesting environments for both in summer and in winter to model the effect of leaves to the propagating channel. Proper channel sounder equipment is therefore also needed. Due to the high investment costs of the measuring equipment, other possibilities (e.g. renting) should be investigated. It might also be possible to further develop the existing sounder equipment of the Radio laboratory of Helsinki University of Technology in such a way that it is also suitable for 2.4 GHz measurements. An example of suitable commercial radio channel sounder equipment is the PROPSound by Elektrobit Group.

After the impulse response measurements, a lot of statistical post-processing of the measurement results needs to be carried out. For example, Matlab is a suitable tool for processing the raw data and acquiring the other system functions and characteristics of the linear time-variant radio channel. With the help of these tools, reliable and thorough wideband channel models for different outdoor environments can be achieved. The model can then be compared with existing large-scale and small-scale channel models.

Once the channel information is available some more interesting research can begin. IEEE 802.11b WLAN behaviour in a channel with a delay spread larger than 1 μs (or 727 ns) is one interesting subject, due to the WLAN receiver's problems of taking into account components arriving later than this time without the use of advanced countermeasures. Simulations using measured channel

information can be used to analyse the behaviour of WLAN receivers if the percentage amount of energy received after 1 μs (of 727 ns) is increased to see the real impact of such a channel on system performance and quality. Also different types of WLAN receivers can be developed with the help of simulations based on reliable channel information.

References

[Ame53] W.S. Ament, "Toward a theory of reflection by a rough surface", *Proceedings of the IRE*, Vol. 41, No. 1, January 1953, pp. 142-146

[Bel63] P.A. Bello, "Characterization of randomly time-variant linear channels", *IEEE Trans.*, Vol CS-11, No 4, December 1963, pp. 360-393

[Bro95] P.G. Brown, C.C. Constantinou, "Prediction of radiowave propagation in urban microcell environment using ray-tracing methods", *Antennas and propagation*, IEE Conference Publication No. 407, April 1995, pp. 373-376

[BVS] BVS, "*Yellowjacket 802.11b W-LAN Analysis - System manual version 2.0*", Berkeley Varitronics Systems Inc., 22 pp.

[Che02] C.K. Cheung, J.E.L. Hollis, "A new 3-D ray-tracing propagation model", *3G Mobile communications technologies*, IEE Conference Publication No. 489, May 2002, pp. 201-205

[Chh96] H.S. Chhaya, "Performance of asynchronous Data Transfer Methods of IEEE 802.11 MAC Protocol", *IEEE Personal Communications*, October 1996, pp. 8-15

[Cla68] R.H. Clarke, "A statistical theory of mobile-radio reception", *The Bell System Technical Journal*, July-August 1968, pp. 957-1000

[COS01] COST Action 259 Final Report, "*Wireless Flexible Personalised Communications*", ISBN 0-471-49836X, Wiley, London, 462 pp., 2001

[COS99] COST Action 231E Final Report, "*Digital mobile radio towards future generation systems*", ISBN 92-828-5416-7, European Communities, Belgium, 474 pp., 1999

[Cox72] D.C. Cox, "Delay Doppler Characteristics of Multipath Propagation at 910 MHz in a Suburban Mobile Radio Environment", *IEEE Transactions on Antennas and Propagation,* Vol. AP-20, No. 5, September 1972, pp. 625-635

[Cro97] B.P. Crow, "IEEE 802.11 Wireless Local Area Networks", *IEEE Communications Magazine* September 1997, pp. 116-126

[ETS01] ETSI EN 300 328-1 "*Electromagnetic compatibility and Radio spectrum Matters (ERM); Wideband Transmission systems; Data transmission equipment operating in the 2,4 GHz ISM band and using spread spectrum modulation techniques; Part 1: Technical characteristics and test conditions*", V1.3.1, ETSI, 34 pp., 2001

[ETS93] ETSI GSM 05.05 "*European digital cellular telecommunication system (phase 2); Radio transmission and reception*", V4.6.0, ETSI, 31 pp., 1993

[Gas02] M.S. Gast "*802.11 Wireless Networks: The Definitive Guide*", ISBN: 0-596-00183-5, O´Reilly, Sebastopol, USA, 443 pp. 2002

[Gru] P. Grupta, "*WLAN: Digesting the 802.11 Alphabet Soup*", Courtesy of TechRepublic, http://techrepublic.com, http://people.cs.uct.ac.za/~schetty/WLAN-described.pdf, 3 pp., last visited 17th of June 2003.

[Har99a] D. Har, H.H. Xia, H.L. Bertoni, "Path-Loss Prediction Model for Microcells", *IEEE Transactions on Vehicular Technology*, vol. 48, no. 5, September 1999, pp. 1453-1462

[Har99b] D. Har, A.M. Watson, A.G. Chadney, "Comment of Diffraction Loss of Rooftop-to-Street in COST231-Walfisch-Ikegami Model", *IEEE Transactions on Vehicular Technology*, Vol 48, No 5, September 1999, pp. 1451-1452

[Hea00] A. Healey,C.H. Bianchi, K. Sivaprasad, "Wideband outdoor channel sounding at 2.4 GHz", "*Antennas and Propagation for Wireless Communications*", 2000 IEEE-APS Conference on , 6-8 Nov. 2000 pp. 95-98

[Ho02] Ming-Ju Ho, "RF Challenges for 2.4 and 5 GHz WLAN Deployment and Design", *Wireless Communications and Networking Conference*, 2002. WCNC2002. 2002 IEEE, Volume: 2, 2002 Page(s): 783-788, vol.2

[Hol00] P.D. Holm, "A new Heuristic UTD Diffraction Coefficient for Nonperfectly Conducting Wedges", *IEEE Transactions on Antennas and Propagation*, vol. 48, no. 8, August 2000 pp. 1211-1219

[IEE99a] IEEE 802.11 Std, "*Wireless LAN Medium Access Control (MAC) and Physical Layer (PHY) Specifications*", ISO/IEC 8802-11, IEEE, 512 pp., 1999

[IEE99b] IEEE 802.11b Std, "*Wireless LAN Medium Access Control (MAC) and Physical Layer (PHY) specifications: Higher-Speed Physical Layer Extension in the 2.4 GHz Band*" ISO/IEC 7498-1, IEEE, 96 pp. 1999

[ITU03a] ITU-R Recommendation P.1411-2, "*Propagation data and prediction methods for the planning of short-range outdoor radiocommunication systems and radio local area networks in the frequency range 300 MHz to 100 GHz*", ITU-R, 17 pp., 2003

[ITU03b] ITU-R Recommendation P.833-4, "*Attenuation in vegetation*", ITU-R, 7 pp., 2003

[ITU03c] ITU-R Recommendation P.526-8, "*Propagation by diffraction*", ITU-R, 22 pp., 2003

[ITU97] ITU-R Recommendation M.1225, "*Guidelines for valuation of radio transmission technologies for IMT-2000*", ITU-R, 60 pp., 1997

[Jin93] J. Jin, "*The finite element method in electromagnetics*" ISBN 0-471-58627-7, Wiley, London, 442 pp., 1993

[Kal98] K. Kalliola, J. Laurila, M. Toeltsch, K. Hugl, P. Vainikainen, E. Bonek, "Dynamic Wideband Measurement of Mobile Radio Channel with Apadtive Antennas", *Proc. 48th IEEE Vehicular Technology Conference (VTC´98)*, Ottawa, Ontario, Canadam May 18-21, 1998, pp. 21-25

[Kee02] I. Keene, "*The ABCs of 802.11 standards*", ZDnet, http://techupdate.zdnet.com/techupdate/stories/main/0,14179,2857227-3,00.html, March 2002, last visited 17th of June 2003.

[Kiv99] J. Kivinen, T.O. Korhonen, P. Aikio, R. Gruber, P. Vainikainen, S.-G. Häggman, "Wideband Radio Channel Measurement System at 2 GHz", *IEEE Transactions on instrumentation and measurement*, Vol. 48, No. 1, February 1999, pp. 39-44

[Lin85] I. Lindell, "*Radioaaltojen eteminen (Radio wave propagation, in Finnish)*", ISBN 951-672-227-X, 4th ed., Otatieto Oy, Helsinki, 261 pp., 1996

[Lit96] J.Litva, C. Wu, A. Ghaforian, "Use of FDTD for simulating the angle of arrival and time delay of signals propagating in indoor environments", *Electronic letters*, Vol. 32, No. 10, May 1996, pp. 930-932

[Luc00] Lucent Technologies, "*Getting Started Guide of Orinoco WLAN PC Card*", Lucent Technologies Inc., USA, 65 pp., 2000

[Mes99] H. Meskanen, "*Lift car propagation analysis and modeling with FDTD simulations and measurements*", Licentiate's thesis, Helsinki University of Technology, Communication laboratory, Espoo, 1999, 92 pp.

[Nik92] K. Nikoskinen, "*Sähkömagnetiikan kaavoja (Equations for electromagnetism, in Finnish)*", ISBN 951-672-142-7, Otatieto Oy, Helsinki, 124 pp., 1992

[OHa99] N. O´Hara, A. Petrick, "*IEEE 802.11 Handbook – A Designer's Companion*", ISBN 0-7381-1855-9, Institute of Electrical and Electronics Engineers, Inc., New York, 174 pp., 1999

[Par00] J.D. Parsons, "*The mobile radio propagation channel*", 2nd edition, ISBN 0-471-98857-X, Wiley, London, 418 pp., 2000

[Pro95] J.G. Proakis, "*Digital Communications*", 3rd edition, ISBN 0-07-113814-5, McGraw-Hill Book Co., Singapore, 928 pp., 1995

[Rap96] T.S. Rappaport, "*Wireless Communications*", ISBN 0-13-461088-1, Upper Saddle River (NJ), Prentice Hall PTR, 641 pp., 1996

[Rog02] N.C. Rogers, "*A Generic Model of 1-60 GHz Radio Propagation through Vegetation – Final Report*", QINETIQ/KI/COM/CR020196/1.0, UK, 152 pp., May 2002

[Rut97] K. Ruttik, M. Honkanen, M. Hall, T. Korhonen, V. Porra, "A wideband radio channel model for simulations of the chaotic communication systems", *Proceedings on the 1997 European Conference on Circuit Theory and Design ECCTD´97*", Vol. 1, Budapest, Hungary, 1997, pp. 302-305,

[San01] A. Santamaria, F. López-Hernánder, "*Wireless LAN standards and applications*", ISBN 0-89006-943-3, Artech house inc., Norwood, USA, 234 pp., 2001

[Sch94] K.R. Schaubach, N.J. Davis IV, "Microcellular radio-channel propagation prediction", *IEEE Antennas and propagation magazine*, Vol. 36, No. 4, August 1994, pp. 25-34

[She00] X.Q. Sheng, E.K-N. Yung, C.H. Chan, "Scattering from large body with cracks and cavities by the fast and accurate finite-element boundary-integral method", *IEEE Transactions on antennas and propagation*, Vol. 48, No. 8, August 2000, pp. 1153-1160

[Taf95] A. Taflove, "*Computational electrodynamics – The Finite-Difference Time-Domain Method*", ISBN 0-89006-792-9, Arctec house Inc., Norwood, 599 pp.

[Vie03] Viestintävirasto, "*Radiotaajuuksien käyttösuunnitelma 470 – 3400 MHz*", http://www.ficora.fi/suomi/radio/Taulukko3.htm, last visited 11th of June 2003.

[Vuo01] L. Vuokko, "*Radioaaltojen etenemismekanismit kaupunkiympäristössä 2 GHz:n taajuusalueella (Radio wave propagation mechanisms in city environment at 2 GHz frequency range, in Finnish)*", Master's thesis, Helsinki University of Technology, Radio Laboratory, Espoo 2001, 71 pp.

[Woo99] G. Woodward, I. Oppermann, J. Talvitie, "*Outdoor-Indoor Temporal & Spatial Wideband Channel Model for ISM Bands*" Vehicular Technology Conference, 1999. VTC 1999 - Fall. IEEE VTS 50th, Volume: 1, 19-22 Sept. pp. 136 -140

Appendix A: GSM channel models

Table A-1 Tap setting for hilly terrain environment

Tap	Channel A		Channel B		Doppler spectrum
	Relative delay [μs]	Avg. power [dB]	Relative delay [μs]	Avg. power [dB]	
1	0.0	-10.0	0.0	-10.0	Classical
2	0.1	-8.0	0.2	-8.0	Classical
3	0.3	-6.0	0.4	-6.0	Classical
4	0.5	-4.0	0.6	-4.0	Classical
5	0.7	0.0	0.8	0.0	Classical
6	1.0	0.0	2.0	0.0	Classical
7	1.3	-4.0	2.4	-4.0	Classical
8	15.0	-8.0	15.0	-8.0	Classical
9	15.2	-9.0	15.2	-9.0	Classical
10	15.7	-10.0	15.8	-10.0	Classical
11	17.2	-12.0	17.2	-12.0	Classical
12	20.0	-14.0	20.0	-14.0	Classical

Table A-2 Tap setting for urban area

Tap	Channel A		Channel B		Doppler spectrum
	Relative delay [μs]	Avg. power [dB]	Relative delay [μs]	Avg. power [dB]	
1	0.0	-4.0	0.0	-4.0	Classical
2	0.1	-3.0	0.2	-3.0	Classical
3	0.3	0.0	0.4	0.0	Classical
4	0.5	-2.6	0.6	-2.6	Classical
5	0.8	-3.0	0.8	-3.0	Classical
6	1.1	-5.0	1.2	-5.0	Classical
7	1.3	-7.0	1.4	-7.0	Classical
8	1.7	-5.0	1.8	-5.0	Classical
9	2.3	-6.5	2.4	-6.5	Classical
10	3.1	-8.6	3.0	-8.6	Classical
11	3.2	-11.0	3.2	-11.0	Classical
12	5.0	-10.0	5.0	-10.0	Classical